Systems-level analysis of monocyte responses in inflammatory bowel disease identifies IL-10 and IL-1 cytokine networks that regulate IL-23

Dominik Aschenbrenner[1]*, Maria Quaranta[1,8]*, Soumya Banerjee[1,2,9], Nicholas Ilott[2], Joanneke Jansen[1,7], Boyd A. Steere[3], Yin-Huai Chen[1], Stephen Ho[3], Karen Cox[3], Oxford IBD Cohort Investigators[1], Carolina V. Arancibia-Cárcamo[1], Mark Coles[2], Eamonn Gaffney[7], Simon Travis[1], Lee A. Denson[4], Subra Kugathasan[5], Jochen Schmitz[3], Fiona Powrie[2], Stephen Sansom[2]*, and Holm H. Uhlig[1,6]*

Author affiliation

[1] Translational Gastroenterology Unit, NIHR Oxford Biomedical Research Centre, John Radcliffe Hospital, University of Oxford, Oxford, UK.

[2] Kennedy Institute of Rheumatology, University of Oxford, Oxford, UK.

[3] Immunology Translational Sciences; Lilly Research Laboratories. Eli Lilly and Company Lilly Corporate Center, Indianapolis IN 46285, USA.

[4] Division of Pediatric Gastroenterology, Hepatology and Nutrition, Cincinnati Children's Hospital Medical Center, Cincinnati, Ohio, USA.

[5] Division of Pediatric Gastroenterology, Emory University School of Medicine, Atlanta, Georgia, USA.

[6] Department of Paediatrics, University of Oxford, Oxford, UK.

[7] Wolfson Centre for Mathematical Biology, University of Oxford, Oxford, UK.

Current addresses:

[8] IBD Center, Laboratory of Gastrointestinal Immunopathology, Humanitas Clinical and Research Center, Milan, Italy

[9]Department of Psychology, Downing Street, University of Cambridge, Cambridge, UK

*These authors contributed equally to this work

Corresponding author:

Holm H. Uhlig (holm.uhlig@ndm.ox.ac.uk), Translational Gastroenterology Unit, Experimental Medicine, University of Oxford, John Radcliffe Hospital Oxford, OX3 9DU, UK. Phone: 0044 1865 8 57963

Abstract

Dysregulated intestinal immune responses are the cause of inflammatory bowel diseases (IBD). Using single-cell and bulk transcriptomic approaches we investigate the responses of monocytes and peripheral blood mononuclear cells to multiple stimuli and relate those to transcriptional responses in the inflamed intestine. We identify auto- and paracrine sensing of IL-1α/β and IL-10 regulation as key signals that control the development of inflammatory IL-23-producing monocytes. Uptake of whole bacteria induces IL-10 resistance and favours IL-23 secretion. IL-1α/β^{+}CD14^{+} monocyte signatures are enriched in patients with ulcerating intestinal inflammation and resistance to anti-TNF therapy. In contrast, IL-23 and tumour necrosis factor expression in the absence of this inflammatory monocyte signature was associated with homeostatic lymphocyte differentiation explaining why IL-23 and TNF expression alone are poor predictors for IBD activity. Gene co-expression analysis assists the identification of IBD patient subgroups that might benefit from IL-23p19 and/or IL-1α/IL-1β-targeting therapies.

Introduction

The pathogenesis of inflammatory bowel disease (IBD), that include Crohn's disease (CD) and ulcerative colitis (UC) and IBD unclassified (IBDu) is caused by dysregulated innate and adaptive immune responses that drive chronic relapsing tissue inflammation[1]. Genetic studies suggest a complex polygenic inheritance driven by defective innate and adaptive antimicrobial immunity with dysregulated Th17 responses[1,2]. IL-23 signalling and T-helper (Th) 1/Th17 immunity are significant mediators of intestinal inflammation as indicated by genetic variants in *IL23R* encoding the IL-23 receptor[3] as well as *RORC*, *STAT3*, *IRF5*, *IL1R1*, *IL6ST*, *IL12B, TYK2, IL21, JAK2, IFNG, SMAD3* and *CCR6*[4,5]. Studies in both mice and humans suggest a central role of monocytes, macrophages and dendritic cells, that produce IL-23 in response to bacteria- and fungi-derived microbial stimuli and drive Th1 and Th17 differentiation in the pathogenesis of intestinal inflammation[6-9]. In addition to a role of pro-inflammatory and anti-inflammatory cytokine networks[10], mouse models as well as human Mendelian disorders highlight the essential role of IL-10 signalling in controlling inflammatory cytokine responses. Therapeutic approaches that target the pro-inflammatory arm of the immune system by blocking cytokine signalling or by affecting intestinal cell migration are effective in subgroups of patients with IBD[8]. Mice that lack IL-23p19 are protected from developing colitis in innate as well as lymphocyte replete models of intestinal inflammation induced by IL-10 signalling defects, bacterial colonisation or innate immune stimulation *via* the anti-CD40[7,11]. Blockade of IL-23p19 and IL-12p40 showed therapeutic benefit for patients with CD[12,13].

To predict genetic susceptibility or disease course, individual loci and genetic risk scores[14,15] as well as gene expression signatures or transcriptomic scores of peripheral $CD8^+$ T cells[16] , peripheral blood[17] or intestinal tissue[18] are emerging patient stratification strategies in IBD. Membrane-bound TNF[19] and IL-6/Oncostatin M (OSM) associated cytokines[18] predict anti-

TNF non-response. However, transcriptional signatures that implement IL-23 expression have not been described.

Personalised medicine targeting the IL-23 axis requires an understanding of the cellular sources, networks and regulation of IL-23 production. There are essential questions that need to be resolved: How are pro- and anti-inflammatory cytokines co-regulated within monocytes during tissue inflammation and what are the key drivers of IL-23 expression? In light of the emerging evidence of the dual role of cytokines such as TNF and IL-17A for protective host response and tissue inflammation an understanding of the potential role of host protective and pathogenic IL-23 responses in the intestine is also needed.

Here we investigate the regulation of IL-23 in a modelled response towards relevant microbe-derived stimuli in peripheral blood cells, describe distinct monocyte subsets that express IL-23 and identify IL-1-signalling as the key cytokine for the differentiation of an IL-23-producing monocyte subset. We identify an IL-23^{+}IL-1^{+} expression signature in intestinal tissue transcriptomes of patients with IBD and distinguish this from a homeostatic signature associated with IL-23 in non-inflamed intestine.

Results

Transcriptomics of *in vitro* stimulated peripheral blood mononuclear cells (PBMC) identifies key modulators of inflammatory cytokines

We systematically investigated the transcriptomic response pattern of PBMC from 41 patients with IBD (**Supplementary Table 1**) to IBD relevant stimuli that target different aspects of innate and adaptive immune cell responses. Lipopolysaccharide (LPS), muramyl-dipeptide (MDP), T cell receptor and co-stimulation (αCD3/αCD28 coated beads) and IL-10 signalling blockade were used alone or in combination based on the concept that innate pathogen recognition receptor responses (in particular NOD2[14] and TLR4[20]), T cell responses and IL-10 signalling defects are implicated by multiple genetic IBD susceptibility loci and Mendelian forms of IBD[21]. We performed microarray gene expression analysis of all conditions at 16 hours following stimulation (LPS, L18MDP and αCD3/αCD28 coated beads) in presence or absence of IL-10 receptor blocking antibodies **(Figure 1a; Supplementary Fig. 1a and Supplementary Table 2)**. We then identified stimulus-specific and shared gene expression signatures and enriched gene ontology categories *via* differential gene expression analysis (**Figure 1b, Supplementary Fig. 1d and 1e**). LPS, L18MDP, and αCD3/αCD28 coated beads induced 319, 187 and 312 genes respectively with 109, 19, and 175 genes being specific to each of the respective conditions (BH adjusted $p < 0.05$, $| fc | \geq 1.5$; **Figure 1b**). Geneset over-representation analysis indicated that IL-10 signalling was among the pathways associated with all conditions, and over 50% of genes regulated by all three stimuli were associated with IL-10 signalling (**Supplementary Fig. 1e**).

We therefore investigated the role of IL-10 signalling during LPS, L18MDP, and αCD3/αCD28 stimulation by blocking IL-10 signalling with an anti-IL-10R antibody. In total 36 genes were up- and 29 genes down-regulated ($|fc| > 1.5$, BH-adjusted $p < 0.05$; **Figure 1c and 1d; Supplementary Table 3).** After LPS stimulation, IL-10R blockade induced 34

genes (including *IFNG*, *IL23A*, *CXCL10*, *IL19* and *IL36G*) and repressed 27 genes (including *CD163* and *VCAN,* **Supplementary Table 3**, **Figure 1c and 1d**). After L18MDP stimulation IL-10R blockade induced 3 and repressed 5 genes and after αCD3/αCD28 stimulation IL-10R blockade induced 14 and repressed 3 genes. Blockade of IL-10-induced genes associated with Rheumatoid arthritis (RA) and IBD, Toll-like receptor signalling, IFN-γ-signalling and the NFκB signalling pathway, and repressed genes that showed enrichments for extracellular matrix proteoglycans, scavenging of heme from plasma, dectin-2 family proteins and protozoan parasite invasion of the intestinal epithelium (amoebiasis) **(**BH adjusted $p < 0.05$**, Supplementary Fig. 2a and 2b).** We validated these results at the level of gene expression by RT-qPCR for *IL23A* and *IFNG* (**Supplementary Fig. 1b and 1c**). To investigate the regulation of secreted proteins by IL-10, we analysed cell culture supernatants after 16 hours stimulation **(Figure 2a and Supplementary Fig. 2c)**. Among the 41 proteins tested, IL-10 blockade significantly up-regulated 6 LPS-induced factors (IL-23p19, GM-CSF, IL-1α, IL-12p70, IL-12p40 and IFN-γ; **Figure 2a**) (BH Adjusted $p < 0.05$, $| fc | \geq 4$-fold). Compared to control, LPS stimulation resulted in a mean 85.23-fold induction (mean concentration control: 3.30 pg/ml, mean concentration LPS 135.98 pg/ml) of IL-23 (BH adjusted $p < 0.05$) while combined LPS and anti-IL-10R treatment induced a mean 2,544.95-fold increase (mean concentration LPS and anti-IL-10R 4737.57 pg/ml) IL-23 secretion (BH adjusted $p < 0.05$) (**Figure 2b**).

We next sought to understand the kinetics and cellular sources of IL-10 regulated LPS-responsive cytokines within the complex PBMC mixture. We quantitated IL-1α, IL-1β, IL-4, IL-6, IL-10, IL-12p40, IL-13, IL-17A, IL-23p19, GM-CSF, IFN-γ and TNF production in monocytes, NK cells, $CD4^+$ T cells and $CD8^+$ T cells by intracellular flow cytometry in patients with IBD and healthy donors (HD) PBMCs (**Supplementary Fig. 3a and 3b**). To capture the early and late phase of cytokine production we analysed cells at 6 and 16 hours

following stimulation. At both time points of stimulation, $CD14^+$ monocytes were the major source of IL-10, and also produced IL-1α, IL-1β, IL-6 and TNF (**Supplementary Fig. 3a and 3b**). $CD4^+$ T cells contributed to the early cytokine response *via* expression of IFN-γ, IL-17A, GM-CSF and TNF, while $CD8^+$ T cells produced IFN-γ and TNF (**Supplementary Fig. 3a and 3b**). NK cells contributed to the cytokine response by production of IFN-γ and TNF only at the late time point. Interestingly, following 16 hours of stimulation monocytes still produced IL-1α and IL-1β while IL-6, TNF and IL-10 expression were reduced. All these cytokines were increased when cells were stimulated with LPS and anti-IL-10R. IL-23 (IL-12p40$^+$IL-23p19$^+$) and IL-12 (IL-12p40$^+$IL-23p19$^-$) expression were selectively increased in $CD14^+$ relative to $CD14^-$ leukocytes after IL-10 receptor blockade (**Figure 2c, 2d and 2e**). These results were confirmed in PBMC obtained from HDs **(Supplementary Fig. 3c, 3d and 3e)**. Together, these results demonstrate that IL-10 signalling regulates IL-23 (IL-12p40$^+$IL-23p19$^+$) production in a subset of $CD14^+$ monocytes (IBD mean = 3.03 % (95% CI of the mean: lower = 1.11, upper = 4.96); HD mean = 5.32 % (95% CI of the mean: lower = 3.51, upper = 7.14)).

Single cell sequencing identifies inflammatory IL-10 regulated monocyte phenotypes

FACS analysis suggested the presence of unknown functional heterogeneity within the population of stimulated $CD14^+$ monocytes (see *e.g.* **Figure 2c).** To characterise the LPS-induced and IL-10-regulated transcriptional profile of monocytes subsets, and to differentiate population-wide transcriptional changes from subset-specific responses we performed single cell RNA-sequencing of $CD14^+$ MACS-sorted monocytes from HD**.** Data from unstimulated, LPS-stimulated or LPS and anti-IL-10R-treated cells from a common donor were subject to unsupervised graph-based clustering and visualized on a t-Distributed Stochastic Neighbor Embedding (tSNE) plot (**Figure 3a)**. Among the 8 clusters of monocytes that were detected,

2 clusters emerged after LPS stimulation and 3 additional clusters largely comprised of LPS and anti-IL-10R stimulated cells **(Figure 3a and 3b)**.

The eight clusters showed discrete gene expression **(Figure 3c)** and were enriched for biological processes suggestive of different functional specialisations **(Supplementary Fig. 4a)**. The majority of unstimulated monocytes were lysozyme^{+} (*LYZ*), *CD52*$^{+}$ (*CAMPATH1*), and *FCN1*$^{+}$ expressing *CD14*^{high} monocytes (cluster 0 – unstimulated, classical monocytes), while a minority of unstimulated monocytes displayed a *CD52*$^{+}$, *FCN1*$^{+}$, *CD16*$^{+}$ (*FCGR3A*) *CD14*^{low} phenotype (cluster 7 – unstimulated, non-classical monocytes). Two clusters of cells that emerged following LPS stimulation were comprised of *IL1B*$^{+}$ cells. The first showed expression of *CD14* and was enriched for genes associated with "T cell tolerance induction" (cluster 1 – LPS-stimulated), while the second displayed high *CD300E* and *CD163* expression and an enrichment for "monocyte activation" genes (cluster 2 – LPS-stimulated). The three additional monocyte phenotypes that appeared upon combined LPS stimulation and IL-10R blockade were demarcated by (i) high expression of type 1 interferon responsive genes (*e.g. IFIs*, *IFITs*, *ISGs*, *OASs, IRFs*) and genes linked to antigen processing and presentation (*e.g. B2M*, *CCR7*, *HLA, CD74*) (cluster 3 – LPS and anti-IL-10R, called IFN-induced monocytes); (ii) high expression of *ITGAX* and enrichment for genes associated with "superoxide generation" and "positive regulation of neutrophil activation" (cluster 6 – LPS and anti-IL-10R, called microbicidal monocytes) and (iii) expression of pro-inflammatory genes including (*IL1B*, *IL6*, *IL23A*, *CCL20* and *PTGS2*) and enrichment of genes associated with "Th17 cell lineage commitment", "positive regulation of acute inflammatory response" and "interferon gamma production" (cluster 4 – LPS and anti-IL-10R; called IL-23^{+} inflammatory monocytes). These three phenotypes in LPS-stimulated anti-IL-10R-treated monocytes were replicated in a second donor (**Supplementary Fig. 4b**).

Interestingly, while *IL23A* and *IL1R1* were expressed in a cluster-specific manner under the "hyper-inflammatory" LPS and anti-IL-10R condition, *IL10, IL10RA* and *IL10RB* as well as *IL1A/IL1B* mRNA showed broader, cross-condition and cross-cluster expression (**Figure 3d**).

IL-10-producing monocytes control differentiation of IL-23-producing monocytes through paracrine signalling.

At the population level, we observed that *IL23A* and *IL10* gene expression, we observed that *IL23A* and *IL10* mRNA expression were strongly correlated (Spearmans' r=0.84, p<0.0001) in PBMC subjected to LPS and IL-10R blockade **(Supplementary Fig 5a)**. These data indicate that *IL10* mRNA expression itself is tightly regulated by IL-10 signalling as part of a negative feedback mechanism. This is unlikely to involve IL-23 signalling since, when stimulated under IL-10 blockade, PBMC expressed IL-10 prior to up-regulating IL-23 **(Supplementary Fig. 3a and 3b and Supplementary Fig. 5b).**

In light of the strong correlation between *IL10* and *IL23A* mRNA expression, we assumed that *IL23A* and *IL10* would be produced by the same cells. However, inspection of the single-cell data suggested that this might not be the case and intracellular flow cytometry confirmed that IL-10 and IL-23 largely originate from distinct cells (**Figure 4a**). This indicates that IL-10 may regulate IL-23 production through a paracrine mechanism in functionally distinct cells. Alternatively, it is possible that *IL10* and *IL23A* mRNA expression might occur sequentially (*i.e.* early IL-10 producer become IL-23 producer) or otherwise in an oscillatory fashion within individual cells. To distinguish between these possibilities, we performed a dual-colour ELISpot using MACS-purified monocytes. In line with a paracrine model where IL-10 producing monocytes regulate IL-23 production in others, we found that IL-10-producing monocytes (blue) were distinct from IL-23-producing monocytes (red) and that double-stained cells were a minority (**Figure 4b and 4c**). These results suggest that IL-10

producing monocytes regulate IL-23 producing cells and demonstrate that the development of IL-23-producing monocytes is not a consequence of local segregation of IL-10 and IL-23 producing monocytes in tissue culture.

Deconvolution of intestinal IL-23 gene expression in intestinal tissue

We next sought to understand the context of IL-23 expression during intestinal inflammation. We compared expression of IL-23 in ileal biopsies from Crohn's disease and non-inflamed controls (HD or UC) in samples from the paediatric RISK cohort[22] (**Figure 5a**). As expected, *IL23A* and *IL12B* were expressed in the Crohn's disease patient samples along with *IL1A*, *IL1B* and *IL6*. However, we also found *IL23A* and *IL12B* expression in non-inflamed control biopsies (**Figure 5a and 5b**) where *IL23A* expression was associated with *TNF* rather than *IL1B* expression (**Figure 5c and 5d**). We therefore performed weighted gene co-expression network analysis (WGCNA)[23] to investigate the possible sources and roles of *IL23A* in the inflamed and non-inflamed intestine (**Supplementary Fig. 6a**). This analysis identified 22 gene expression modules that clustered into six different groups based on the expression of their eigengenes (first principle components) in the RISK cohort patients (**Supplementary Fig. 6a)**. The six groups of modules were distinguished by correlations with (i) diagnosis of CD (5 modules), (ii) diagnosis of CD and *IL23A* expression (5 modules), (iii) *IL23A* expression (4 modules), (iv) non-inflammatory control status and epithelial genes (5 modules), (v) mitochondrial activity (2 modules) and (vi) cell growth (one module) (**Supplementary Fig. 6a, Supplementary Fig. 6b and Supplementary Table 4**).

We found that a prominent "inflammatory cytokine" module was associated with both CD and *IL23A* expression. This module contained key myeloid and stromal markers genes (*CD14, PDPN*), pro-inflammatory cytokines (including *OSM, IL1B* and *IL6)* and Fibroblast activation protein (*FAP*) (**Supplementary Fig. 6b**) in keeping with the emerging concept of a

pathogenic myeloid-stromal cell circuit in IBD[18,24]. Although *IL23A* expression was significantly correlated with this module (r=0.35), *IL23A* expression was most strongly associated with modules characterised by gene ontology categories "immune cell differentiation" (r=0.7) and "lymphocyte differentiation" (r=0.71) and the KEGG pathway "Th17 cell differentiation" (**Supplementary Fig. 6a and 7a**).

Of the modules strongly correlated with *IL23A,* the "immune cell differentiation" module also showed only a weak correlation with CD (r=0.2, p=0.002). It was associated with expression of both myeloid (*CD14)* and lymphoid (*CD79A*, *CD4*) cell markers and included a specific enrichment for "myeloid dendritic cell differentiation" (**Supplementary Fig. 6b and 7a**). In contrast, the strongly *IL23A* correlated "lymphocyte differentiation" module was not correlated with CD. Rather, it showed an expression signature suggestive of lymphoid follicles including individual markers of B and T-cell identity (*CD79A*, *CD4*) and differentiation (*BACH2)*[25,26] (**Supplementary Fig. 6b**) as well as enrichments for gene ontology categories related to lymphoid cell differentiation, proliferation and selection (**Supplementary Fig. 7a**). It also showed high correlation with expression of orthologs of genes associated with murine small intestine lymphoid tissue (SILT) including *IL22RA2*, *ITGAX*[27] as well as with *VCAM1*, which is a marker of lymphoid associated villi in humans (**Supplementary Fig. 6b**).

Overall, these observations suggest dual roles for IL-23 in intestinal inflammation and homeostatic non-inflammatory lymphoid cell differentiation. We therefore sought to understand whether other IL-10 regulated monocyte genes were also associated with disease or homeostatic functions. We correlated the expression of a curated set of IL-10 regulated monocyte genes (35 genes specific to combined LPS and anti-IL-10R stimulation scRNA-seq; **Figure 5e and 5f**; Methods section Identification and characterisation of an IL-10-responsive monocyte gene signature) with the eigengenes for the CD-associated

"inflammatory cytokine" and the non-inflammatory "lymphocyte differentiation" modules in the RISK cohort data. This analysis identified three subsets of the IL-10 regulated monocyte genes (**Figure 5e**). These comprised of (i) genes correlated only with the CD associated "inflammatory cytokine" module (black box, **Figure 5e**), (ii) a set of genes correlated with both the "inflammatory cytokine" and "lymphocyte differentiation" modules (grey box, **Figure 5e**), and (iii) genes correlated with only the non-inflammatory "lymphocyte differentiation" module (green box, **Figure 5e**). The IL-10-regulated genes that correlated with the "inflammatory cytokine" but not the "lymphocyte differentiation" eigengene (black box, **Figure 5e**) showed a significantly superior ability to predict anti-TNF response after 4 to 6 weeks treatment in an independent cohort of patients with UC (UC-cohort GSE12251)[28] and diagnosis of CD in the RISK cohort[22] (**Figure 5f, 5g and 5h, Supplementary Table 5**). By contrast, IL-10-regulated monocyte genes that correlated with "lymphocyte differentiation" but not "inflammatory cytokines", had poorer predictive ability (**Figure 5f, 5g and 5h**). These data therefore identify a subset of IL-10 regulated monocyte-derived genes, including *CXCL1/2*, *IL1A*, *IL1B*, *INHA*, *IL6*, *CCL3/4*, *PTGS2*, *CSF2/3* and *GBP1* that show a highly specific association for disease-associated intestinal inflammation in the RISK cohort. By contrast, cytokines such as IL-23 and TNF are not specific for the inflammatory process suggestive of context-dependent roles in homeostasis and inflammation.
Finally, the observation that genes of the "lymphocyte differentiation" module are significantly enriched in IBD GWAS genes (**Supplementary Fig. 7b**) suggests that the development and function of such lymphoid follicles is relevant for the pathogenesis of IBD.

Monocyte uptake of whole bacteria causes IL-10 resistance and IL-23 secretion

The analysis of gene expression data in the RISK cohort suggests IL-23 expression despite presence of IL-10 in a subset of patients with deep ulcerating IBD in the absence of

Mendelian IL-10 or IL-10R loss of function DNA variants, *i.e.* functional IL-10 resistance. In light of the epithelial barrier defect in ulcerating disease that predisposes to bacterial translocation, we tested whether direct contact of monocytes with bacteria can induce functional IL-10 resistance. We treated monocytes for 16 hours with heat killed *Salmonella typhimurium* or *Escherichia coli* strain Nissle. Interestingly, monocytes produced IL-23 and IL-10 upon stimulation (**Figure 6a and 6b**) reminiscent of LPS stimulation in presence of IL-10R blockade. The cellular dichotomy of IL-23 and IL-10 production was maintained under these conditions (**Figure 6b**). To assess IL-10 responsiveness in previously stimulated monocytes we extensively washed cell cultures, subsequently exposed those to recombinant human IL-10 and evaluated phosphorylation of signal transducer and activator of transcription (STAT) 3 (**Figure 6c**). Indeed, bacterial stimulation was associated with an increased proportion of cells that did not respond to IL-10 (**Figure 6d and e**). These results demonstrate that monocyte encounter of whole bacteria induces a state of IL-10 resistance.

IL-1α and IL-1β are essential for monocyte IL-23 production

The regulation of monocyte-derived *IL23A* and *IL10* at the mRNA and protein level suggested that IL-23 and IL-10 co-regulate each other at least partially *via* additional factors (likely cytokines). We therefore investigated the functional effects of 11 cytokines (that were co-regulated with IL-23) either by adding those to the tissue culture or blocking their activity by antagonists (**Figure 7a and b, Supplementary Fig. 8a and 8b**). When blocking IL-1R1 signalling, IL-23 production was near completely abolished (**Figure 7a and 7b, Supplementary Fig. 8a and 8b**). Decreased *IL23A* expression was also observed at the gene expression level **(Supplementary Fig. 8c)**. Blocking IL-1β or IL-1α alone had only partial or no effect on IL-23 production indicating that either cytokine can compensate for the absence of the other in driving monocyte IL-23 production (**Figure 7a, Supplementary Fig. 8a**). The

effect of IL-1β on IL-23 expression was context specific, since addition of IL-1β in the presence of anti-IL-10R blockade alone did not induce IL-23 expression **(Supplementary Fig. 8d).** None of the other tested cytokines (GM-CSF, IL-6, IL-11, IL-17A, IL-18, IL-19, IL-23, IL-24, IL-36γ, TNF and Type I Interferon) demonstrated a significant impact on IL-23 production. Although not essential, addition of IFN-γ or IL-12 increased monocyte IL-23 production (**Figure 7a and b, Supplementary Fig. 8a and 8b**).

To investigate the effects of IL-1R1 blockade on individual cytokines and on monocyte clusters, we stimulated PBMC from HDs with combinations of LPS and anti-IL-10R and analysed monocyte metaclusters based on protein expression. We selected 2 to 3 cluster defining proteins (IL-23^{+} inflammatory monocytes defined by IL-23p19, CCL20 and TNF; IFN-induced monocytes by HLA-DR and IDO-1; microbicidal monocyte by CCL2, S100A8 and CD14; and apoptotic monocytes by RPS6 and SPINK-1, respectively). In line with the single cell mRNA sequencing experiments, we identified the predicted clusters associated with LPS and combined LPS and anti-IL-10R stimulation **(Figure 7c, gating strategy outlined in Supplementary Fig. 8e)**. Blockade of IL-1R1 specifically inhibited the development of IL-23-producing monocytes while other monocyte clusters remained largely unaffected **(Figure 7c and d).** Importantly, monocyte IL-23 production induced by uptake of whole bacteria was similarly dependent on IL-1R1 signalling (**Supplementary Fig. 9a and 9b**) suggesting that IL-23 is downstream of IL-1 signalling in the context bacteria-induced functional IL-10 signalling defects.

A mathematical model of IL-23 regulation in monocytes

To investigate the impact of cytokine networks on monocyte IL-23 production in more detail we analysed the effects of cytokines up-stream of IL-23. We generated a mathematical model of ordinary differential equations describing the interactions of monocyte-produced IL-23,

TNF, IL-1α, IL-1β, IL-6, and IL-10 at the 16-hour time point, utilising the 1750 experimental data points of PBMC stimulation conditions. This first required identifying an initial set of possible cytokine interactions, *i.e.* changes in cytokine production after addition or blockade of a cytokine (FDR corrected paired Wilcoxon test, **Figure 8a**). Then, to determine which of the measured effects were independent of interactions between the other measured cytokines and to quantify the simultaneous effects of the various cytokines in the network, we modelled all feasible network configurations, noting that most of the $n=2^{31}-1$ configurations could be excluded a priori. We identified a single optimal network describing the core network dynamics by ranking the models based on their fit to the data using the Akaike information criterion (**Figure 8b**). In keeping with our previous findings, the model predicts IL-10 signalling to negatively regulate IL-23 and identifies IL-1β as a key upstream regulator (with IFN-γ as an amplifier) of pro-inflammatory IL-1α, IL-6 and IL-23 expression.

To confirm these predictions, we investigated the effect of IL-1R1 blockade on IL-23 expression in the context of genetic deficiency of IL-10 signalling. We stimulated PBMC obtained from a patient with infantile onset IBD due to an *IL10RA* (**Supplementary Fig. 10a**) or *IL10RB* gene defect (**Supplementary Fig. 10b**). Interestingly, patient-derived monocytes produced IL-23 in response to LPS stimulation alone, indicating the intrinsic defect in IL-10R-dependent regulation, confirmed by the inability of exogenous IL-10 to suppress monocyte IL-1β production. Strikingly, and as predicted by our model, IL-1R1 blockade inhibited monocyte IL-23 production in LPS-stimulated PBMC from IL-10R deficient patients and in the context of IL-10R blockade in HD and patients PBMC (**Supplementary Fig. 10b**). Together, these analyses confirmed IL-10 as the major negative regulator of IL-23 production, while IL-1 signalling (and in particular IL-1β) is essential for IL-23 synthesis in the absence of IL-10 signalling.

Discussion

We identify regulatory circuits that control IL-23 production by inflammatory monocytes. These include failure of paracrine IL-10-mediated control as well as autocrine and paracrine signalling of IL-1α and IL-1β in response to inflammatory stimuli. Indeed, increased IL-23 production can be observed in monocytes from patients with IL-10 signalling defects or experimental blockade of the IL-10 receptor, but also monocytes that respond to whole bacteria express IL-23 as a consequence of acquired IL-10 non-responsiveness. Interestingly, loss of IL-10 responsiveness induces *IL23A* mRNA and IL-23 protein expression only in a small fraction of monocytes that express the IL-1 receptor *IL1R1*. This expression contrasted with pervasive induction of IL-1α and IL-1β expression as well as a broad induction of IL-10 expression in monocytes under the same hyper-inflammatory condition.

Importantly, we demonstrate an IL-1-associated, IL-10-regulated IL-23^{+} inflammatory monocyte response *in vitro* and identify a gene signature of those monocytes that predicts both diagnosis of CD and resistance to anti-TNF treatment in intestinal tissue transcriptomes from patients with IBD. Our analyses also identify potential homeostatic roles of IL-23 in lymphocyte differentiation within mucosa-associated lymphoid tissue (MALT). This highlights a dual role of IL-23 expression in two distinct settings: one *IL23A*-associated signature that is linked with *IL-1*-associated inflammation and Th17 cell differentiation in patients with highly active CD, and another *IL23A*-associated signature that is found in individuals without inflammation. Our data suggest that the source of IL-23 in the context of inflammasome activation and IL-1 production in the inflamed intestine are inflammatory monocytes and CX3CR1^{+}IL-1β^{+} positive macrophages[27,29]. In individuals without intestinal inflammation, the correlated signature suggests an association of *IL23A* expression with MALT that is often hyperplastic in patients of young age[30] and terminal ileal location. In the absence of CD14^{+} monocyte accumulation, *IL23A* is most likely expressed by tissue resident

myeloid cells such as migratory dendritic cells (DC), tolerogenic CD103^{+}DC[31] or macrophages, as is known to be the case in mouse SILT[27]. These results possibly suggest that only subgroups of patients with active disease may benefit from IL-23p19, or possibly IL-1 targeting therapies.

The strong predictive ability of an IL-10 sensitive inflammatory monocyte signature (*CD14*, *IL1A*, *IL1B, OSM*, *PTGS2*, *IL6*, *CCL2/3* and *CXCL1/2*) emphasises a surprising and underestimated extent of IL-10 non-responsiveness in IBD. In those patients inflammation is present despite transcription of IL-10 (patients express large amount of IL-10) and absence of pathogenic variants within the IL-10 receptor (exome sequencing did not reveal Mendelian forms of IL-10 receptor signalling defects in this cohort[32] (data not shown)). Our experiments suggest that direct contact of monocytes with whole bacteria can induce IL-10 resistance that allows co-expression of IL-23 and IL-1. This may explain the presence of a prominent signature of IL-10 non-responsiveness in a subgroup of patients with IBD with active inflammation and compromised intestinal barrier. Alternative mechanisms of reduced responsiveness to IL-10 in patients with IBD have been proposed based on the differential expression of IL-10R1[33]. Our ELISpot experiments suggest that IL-23 expression does not arise from differential spatial clustering of IL-10 or IL-23 secreting monocytes and excludes oscillatory or sequential IL-10 and IL-23 transcription. This suggests that the inflammatory microenvironment drives in parallel several monocyte effector programs and monocyte to macrophage and DC differentiation processes, reminiscent to plasmacytoid dendritic cells (pDC) stimulation with a single stimulus (R848 or CpG) of that induces diverse transcriptional states and cellular functions[34]. Whether the described distinct effector and differentiation programs build on previously imprinted monocyte states or arise as a consequence of stochastic processes that drive distinct self-organising transcriptional programs remains to be established. This is likely to be a biological mechanism to ensure

functional heterogeneity under hyper-inflammatory conditions, when diversity in the host defence towards a range of potential pathogens is beneficial.

Recent studies have applied single cell RNA transcriptomic approaches to identify transcriptional signatures in circulating and tissue human monocytes and macrophages[9,24,35-37] and demonstrated phenotypic and functional diversity in monocyte, macrophage and DC populations also in the human small intestine[38]. We have integrated single cell transcriptomics as well as tissue transcriptomics and transcriptional data from stimulation experiments, to understand the regulation of IL-23 in a subset of monocytes. Our reductionist model is based on the concept that under inflammatory conditions, blood circulating immune cells home into the intestine and are likely to be exposed to trigger(s) that we have applied *in vitro*. We have focused on peripheral monocytes, because those cells are recruited to the gut and differentiate into macrophages in steady state, and into inflammatory monocytes during inflammation. Indeed, under inflammatory conditions, the intestinal tissue resident macrophages that arise from yolk sac are outnumbered by monocytes, monocyte-derived dendritic cells and macrophages that populate this inflammatory niche[39]. Under the impact of M-CSF as well as microflora-induced epithelial factors CX3CR1^{high} macrophages differentiate with pro- and anti-inflammatory properties[40]. During inflammation monocytes differentiate into pro-inflammatory MHC-II-high monocytes and macrophages[41,42]. Those M1 macrophages (as opposed to tissue remodelling and repair associated M2 macrophages in a simplified dichotomy model) have been characterized following *in vitro* differentiation using LPS-stimulation and express IL-12 and IL-23 in response to STAT1-dependent IFN-γ signalling[43].

Our work also demonstrates that, in the absence of explicit spatial information, network-based approaches can help to deconvolve the variance in micro-anatomical heterogeneity that is present between small biopsy samples from complex tissues such as the small intestine.

The critical element that differentiates homeostatic IL-23 and TNF response from hyper-inflammation is the co-expression of a multitude of IL-10-regulated factors, including IL-1α and IL-1β in patients with severe active disease and anti-TNF treatment non-responsiveness. These observations agree with previous findings that anti-TNF therapy non-responsive patients with IBD express high myeloid cell-derived OSM[18]. While *OSM* expression was correlated with inflammatory cytokines including *IL1A*, *IL1B*, *IL11* and *IL6*, it did not show correlation with *IL23A* expression. The association of intestinal *IL23A* expression with both inflammation and homeostatic lymphocyte differentiation provides an explanation for this apparent discrepancy.

Several important points need to be addressed: it is not clear whether the IL-23/IL-1 inflammatory signature in the subgroup of patients reflects a temporal disease activity of ulcerating and penetrating disease or whether this is a subgroup of patients more susceptible to IL-23 targeting therapies in general. It is not clear, whether blockade of IL-23 in patients with non-inflammatory homeostatic IL-23 production might disturb immune homeostasis (akin to *de novo* intestinal inflammation in some patients with anti-TNF therapies, or worsening of intestinal inflammation in patients receiving IL-17A targeting monoclonal antibodies). It is currently not clear whether anti-IL-1R1 blockade will be effective in patients with IBD. Studies in monogenic forms of IBD suggest that IL-1R1 blockade can resolve intestinal inflammation in patients with IL-10 receptor defects[44], mevalonate kinase defects and potentially gain of function NLRC4[45] defects all characterised by increased inflammasome activation and IL-1 secretion. IL-1 blockade will not only affect the monocyte response but will have additional effects on licensing for effector cytokine production of Th1 and Th17 cells[46], Th17 differentiation[47] and IL-10 production within the T cell compartment[48].

Altogether our findings may direct transcriptional diagnostic efforts to guide IL-23p19 targeting therapies and to develop IL-1 targeting therapeutic approaches upstream of IL-23.

Methods

Methods, including statements of data availability and any associated accession codes and references, are available in the online version of the paper.

Author contributions

DA, MQ performed experiments. SB, DA, NI, BAS, JJ and SNS performed bioinformatics analyses. SNS was responsible for design, analysis and interpretation of the single-cell RNA-seq experiments and the network analysis of the RISK cohort data. CVA-C, ST, HHU, TD and SK contributed patient cohort recruitment and analysis. JS, ST, SK, FP, SNS and HHU supervised the study. All authors discussed data and contributed to the manuscript.

Acknowledgments

We thank all patients, volunteers and blood donors for participation in this study. We thank Priya Siddhanathi, James Chivenga, Jennifer Hollis and Sebastian Rogatti Granados for excellent technical assistance, Helen Ferry for flow cytometry support. We thank the Oxford Genomics Centre Single-cell core unit for their technical assistance and support. We like to thank Jon Sedgwick for discussion.

We acknowledge the contribution of the BRC Gastrointestinal biobank (11/YH/0020, 16/YH/0247), which is supported by the National Institute for Health Research (NIHR) Oxford Biomedical Research Centre (BRC). We acknowledge support of the BRC (FP, ST, HHU), the Leona M. and Harry B. Helmsley Charitable Trust (FP, HHU), research grants from the Crohn's & Colitis Foundation of America (LAD, SK, HHU, FP and SP), the COLORS in IBD project via a ESPGHAN network grant (HHU), the Wellcome Trust (FP), the Kennedy Trust for Rheumatology Research (SNS), and to the individual study institutions participating in the RISK study. We thank the Oxford IBD Cohort Investigators** Adam

Bailey, Ellie Barnes, Elizabeth Bird-Lieberman, Oliver Brain, Barbara Braden, Jane Collier, James East, Alessandra Geremia, Lucy Howarth, Satish Keshav, Paul Klenerman, Simon Leedham, Rebecca Palmer, Astor Rodrigues, Alison Simmons, Peter Sullivan. The views expressed are those of the author(s) and not necessarily those of the NHS, the NIHR or the Department of Health.

Disclosure and conflict of interest

This research was funded by the National Institute for Health Research (NIHR) Oxford Biomedical Research Centre (BRC). The views expressed are those of the author(s) and not necessarily those of the NHS, the NIHR or the Department of Health. The study has been supported via a collaborative grant by Eli Lilly. BAS, SH, KC and JS are current or previous employees of Eli Lilly. HHU received research support or consultancy fees from UCB Pharma, Eli Lilly, Boehringer Ingelheim, Pfizer and AbVie. FP has received research support or consultancy fees from GSK, UCB Pharma, Medimmune, Janssen and Eli Lilly. SPLT has been adviser to, in receipt of educational or research grants from, or invited lecturer for AbbVie; Amgen; Asahi; Biogen; Boehringer Ingelheim; BMS; Cosmo; Elan; Enterome; Ferring; FPRT Bio; Genentech/Roche; Genzyme; Glenmark; GW Pharmaceuticals; Janssen; Johnson & Johnson; Lilly; Merck; Novartis; Novo Nordisk; Ocera; Pfizer; Shire; Santarus; SigmoidPharma; Synthon; Takeda; Tillotts; Topivert; Trino Therapeutics with Wellcome Trust; UCB Pharma; Vertex; VHsquared; Vifor; Warner Chilcott and Zeria. SK has received consultancy fees or research support from Abbvie, Allergan, Amgen, Boehringer Ingelheim, ChemoCentryx, Dr Falk Pharma, Ferring, Genentech/Roche, Gilead, GSK, Merck, Mitsubishi Tanabe Pharma, Pharmacosmos, Pfizer, Takeda, and Vifor Pharma

References

1. Uhlig, H. H. & Powrie, F. Translating Immunology into Therapeutic Concepts for Inflammatory Bowel Disease. *Annu. Rev. Immunol.* **36,** 755–781 (2018).
2. Mirkov, M. U., Verstockt, B. & Cleynen, I. Genetics of inflammatory bowel disease: beyond NOD2. *Lancet Gastroenterol Hepatol* **2,** 224–234 (2017).
3. Duerr, R. H. *et al.* A Genome-Wide Association Study Identifies IL23R as an Inflammatory Bowel Disease Gene. *Science* **314,** 1461–1463 (2006).
4. Jostins, L. *et al.* Host-microbe interactions have shaped the genetic architecture of inflammatory bowel disease. *Nature* **491,** 119–124 (2012).
5. de Lange, K. M. *et al.* Genome-wide association study implicates immune activation of multiple integrin genes in inflammatory bowel disease. *Nat Genet* **49,** 256–261 (2017).
6. Hue, S. *et al.* Interleukin-23 drives innate and T cell–mediated intestinal inflammation. *J. Exp. Med.* **203,** 2473–2483 (2006).
7. Uhlig, H. H. *et al.* Differential activity of IL-12 and IL-23 in mucosal and systemic innate immune pathology. *Immunity* **25,** 309–318 (2006).
8. Neurath, M. F. Current and emerging therapeutic targets for IBD. *Nat Rev Gastroenterol Hepatol* **14,** 269–278 (2017).
9. Martin, J. C. *et al.* Single-cell analysis of Crohn's disease lesions identifies a pathogenic cellular module associated with resistance to anti TNF therapy. *bioRxiv* 503102 (2018). doi:10.1101/503102
10. Friedrich, M., Pohin, M. & Powrie, F. Cytokine Networks in the Pathophysiology of Inflammatory Bowel Disease. *Immunity* **50,** 992–1006 (2019).
11. Yen, D. *et al.* IL-23 is essential for T cell–mediated colitis and promotes inflammation via IL-17 and IL-6. *J. Clin. Invest.* **116,** 1310–1316 (2006).
12. Feagan, B. G. *et al.* Induction therapy with the selective interleukin-23 inhibitor risankizumab in patients with moderate-to-severe Crohn's disease: a randomised, double-blind, placebo-controlled phase 2 study. *The Lancet* **389,** 1699–1709 (2017).
13. Sands, B. E. *et al.* Efficacy and Safety of MEDI2070, an Antibody Against Interleukin 23, in Patients With Moderate to Severe Crohn's Disease: A Phase 2a Study. *Gastroenterology* **153,** 77–86.e6 (2017).
14. Cleynen, I. *et al.* Inherited determinants of Crohn's disease and ulcerative colitis phenotypes: a genetic association study. *Lancet* **387,** 156–167 (2016).
15. Lee, J. C. *et al.* Genome-wide association study identifies distinct genetic contributions to prognosis and susceptibility in Crohn's disease. *Nat Genet* **49,** 262–268 (2017).
16. Lee, J. C. *et al.* Gene expression profiling of CD8+ T cells predicts prognosis in patients with Crohn disease and ulcerative colitis. *J. Clin. Invest.* **121,** 4170–4179 (2011).
17. Biasci, D. *et al.* A blood-based prognostic biomarker in IBD. *Gut* gutjnl–2019–318343 (2019). doi:10.1136/gutjnl-2019-318343
18. West, N. R. *et al.* Oncostatin M drives intestinal inflammation and predicts response to tumor necrosis factor-neutralizing therapy in patients with inflammatory bowel disease. *Nat. Med.* **23,** 579–589 (2017).
19. Gaujoux, R. *et al.* Cell-centred meta-analysis reveals baseline predictors of anti-TNFα non-response in biopsy and blood of patients with IBD. *Gut* **68,** 604–614 (2019).
20. Baillie, J. K. *et al.* Analysis of the human monocyte-derived macrophage transcriptome and response to lipopolysaccharide provides new insights into genetic aetiology of inflammatory bowel disease. *PLOS Genet* **13,** e1006641 (2017).
21. Glocker, E.-O. *et al.* Inflammatory Bowel Disease and Mutations Affecting the

Interleukin-10 Receptor. *N Engl J Med* **361,** 2033–2045 (2009).
22. Kugathasan, S. *et al.* Prediction of complicated disease course for children newly diagnosed with Crohn's disease: a multicentre inception cohort study. *The Lancet* **389,** 1710–1718 (2017).
23. Zhang, B. & Horvath, S. A general framework for weighted gene co-expression network analysis. *Stat Appl Genet Mol Biol* **4,** Article17 (2005).
24. Smillie, C. S. *et al.* Rewiring of the cellular and inter-cellular landscape of the human colon during ulcerative colitis. *bioRxiv* 455451 (2018). doi:10.1101/455451
25. Igarashi, K. & Itoh-Nakadai, A. Orchestration of B lymphoid cells and their inner myeloid by Bach. *Curr. Opin. Immunol.* **39,** 136–142 (2016).
26. Richer, M. J., Lang, M. L. & Butler, N. S. T Cell Fates Zipped Up: How the Bach2 Basic Leucine Zipper Transcriptional Repressor Directs T Cell Differentiation and Function. *J. Immunol.* **197,** 1009–1015 (2016).
27. Savage, A. K., Liang, H.-E. & Locksley, R. M. The Development of Steady-State Activation Hubs between Adult LTi ILC3s and Primed Macrophages in Small Intestine. *J. Immunol.* **199,** 1912–1922 (2017).
28. Arijs, I. *et al.* Mucosal gene signatures to predict response to infliximab in patients with ulcerative colitis. *Gut* **58,** 1612–1619 (2009).
29. Shaw, M. H., Kamada, N., Kim, Y.-G. & Nuñez, G. Microbiota-induced IL-1β, but not IL-6, is critical for the development of steady-state TH17 cells in the intestine. *J. Exp. Med.* **209,** 251–258 (2012).
30. Senda, T. *et al.* Microanatomical dissection of human intestinal T-cell immunity reveals site-specific changes in gut-associated lymphoid tissues over life. *Mucosal Immunol* **12,** 378–389 (2019).
31. Longman, R. S. *et al.* CX_3CR1^+ mononuclear phagocytes support colitis-associated innate lymphoid cell production of IL-22. *Journal of Experimental Medicine* **211,** 1571–1583 (2014).
32. Denson, L. A. *et al.* Clinical and Genomic Correlates of Neutrophil Reactive Oxygen Species Production in Pediatric Patients With Crohn's Disease. *Gastroenterology* **154,** 2097–2110 (2018).
33. Nunberg, M. Y. *et al.* Impaired IL-10 Receptor-mediated Suppression in Monocyte From Patients With Crohn Disease. *J. Pediatr. Gastroenterol. Nutr.* **66,** 779–784 (2018).
34. Alculumbre, S. G. *et al.* Diversification of human plasmacytoid predendritic cells in response to a single stimulus. *Nat. Immunol.* 1 (2017). doi:10.1038/s41590-017-0012-z
35. Dixit, A. *et al.* Perturb-Seq: Dissecting Molecular Circuits with Scalable Single-Cell RNA Profiling of Pooled Genetic Screens. *Cell* **167,** 1853–1866.e17 (2016).
36. Villani, A.-C. *et al.* Single-cell RNA-seq reveals new types of human blood dendritic cells, monocytes, and progenitors. *Science* **356,** eaah4573 (2017).
37. Cohen, M. *et al.* Lung Single-Cell Signaling Interaction Map Reveals Basophil Role in Macrophage Imprinting. *Cell* **175,** 1031–1044.e18 (2018).
38. Bujko, A. *et al.* Transcriptional and functional profiling defines human small intestinal macrophage subsets. *J. Exp. Med.* **215,** jem.20170057–458 (2017).
39. Guilliams, M. & Scott, C. L. Does niche competition determine the origin of tissue-resident macrophages? *Nat. Rev. Immunol.* **17,** 451–460 (2017).
40. Stagg, A. J. Intestinal Dendritic Cells in Health and Gut Inflammation. *Front Immunol* **9,** 2883 (2018).
41. Kamada, N. *et al.* Unique CD14+ intestinal macrophages contribute to the pathogenesis of Crohn disease via IL-23/IFN-γ axis. *J. Clin. Invest.* **118,** 2269–2280 (2008).

42. Rivollier, A., He, J., Kole, A., Valatas, V. & Kelsall, B. L. Inflammation switches the differentiation program of Ly6Chi monocytes from antiinflammatory macrophages to inflammatory dendritic cells in the colon. *Journal of Experimental Medicine* **209,** 139–155 (2012).
43. Glass, C. K. & Natoli, G. Molecular control of activation and priming in macrophages. *Nat. Immunol.* **17,** 26–33 (2016).
44. Shouval, D. S. *et al.* Interleukin 1β Mediates Intestinal Inflammation in Mice and Patients With Interleukin 10 Receptor Deficiency. *Gastroenterology* **151,** 1100–1104 (2016).
45. Holzinger, D., Kessel, C., Omenetti, A. & Gattorno, M. From bench to bedside and back again: translational research in autoinflammation. *Nature Reviews Rheumatology* **11,** 573–585 (2015).
46. Jain, A., Song, R., Wakeland, E. K. & Pasare, C. T cell-intrinsic IL-1R signaling licenses effector cytokine production by memory CD4 T cells. *Nat Commun* **9,** 3185 (2018).
47. Acosta-Rodriguez, E. V., Napolitani, G., Lanzavecchia, A. & Sallusto, F. Interleukins 1beta and 6 but not transforming growth factor-beta are essential for the differentiation of interleukin 17-producing human T helper cells. *Nat. Immunol.* **8,** 942–949 (2007).
48. Zielinski, C. E. *et al.* Pathogen-induced human TH17 cells produce IFN-γ or IL-10 and are regulated by IL-1β. *Nature* **484,** 514–518 (2012).
49. Korsunsky, I. Fast, sensitive, and accurate integration of single cell data with Harmony. *bioRxiv* 461954 (2018). doi:10.1101/461954

Fig.1

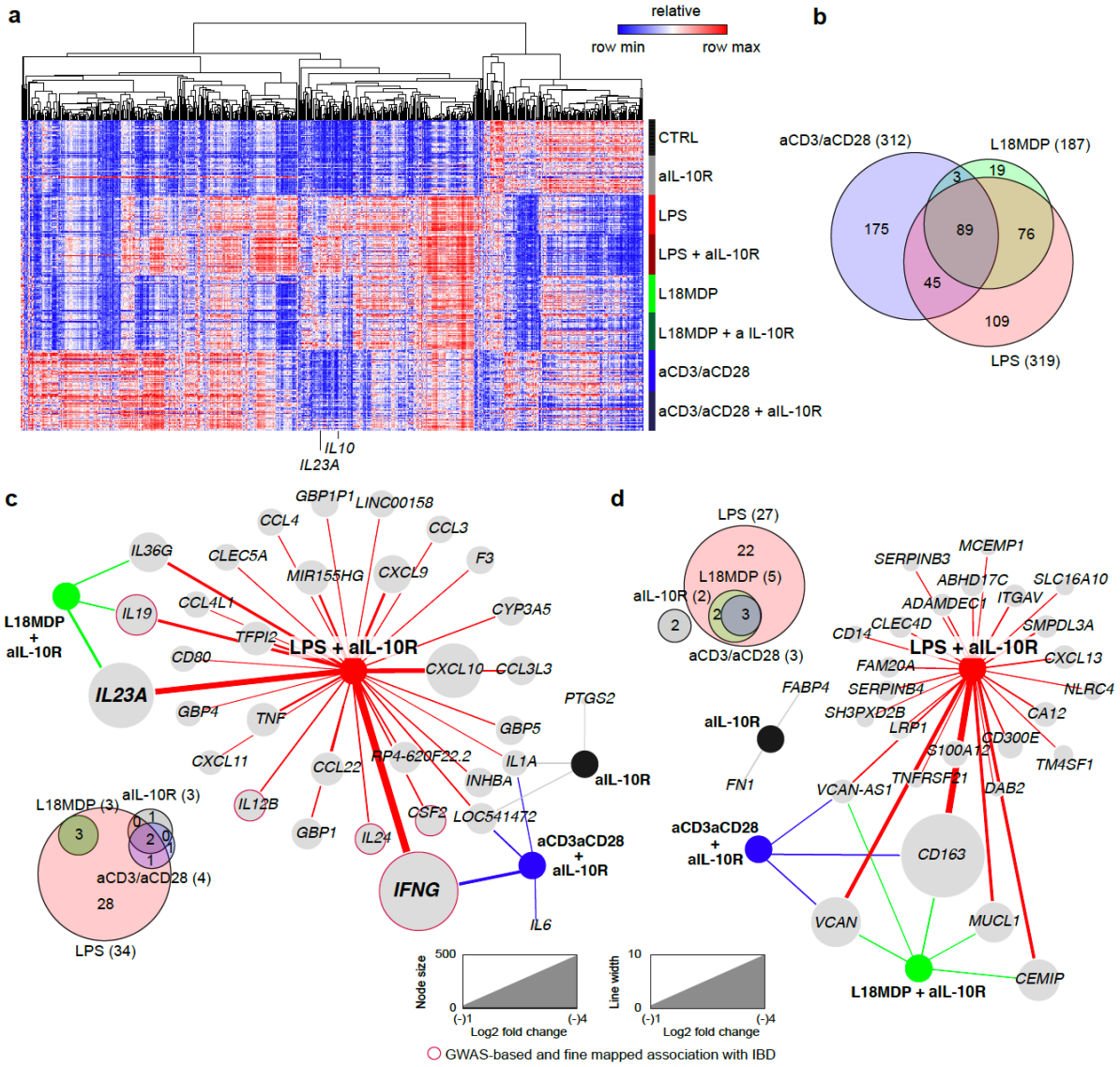
a
relative
row min
row max
CTRL
aIL-10R
LPS
LPS + aIL-10R
L18MDP
L18MDP + a IL-10R
aCD3/aCD28
aCD3/aCD28 + aIL-10R
IL10
IL23A
b
aCD3/aCD28 (312)
L18MDP (187)
LPS (319)
175
3
19
89
76
45
109
c
L18MDP + aIL-10R
IL36G
IL19
IL23A
LPS + aIL-10R
GBP1P1
LINC00158
CCL4
CCL3
CLEC5A
MIR155HG
CXCL9
F3
CCL4L1
TFPI2
CYP3A5
CD80
CXCL10
CCL3L3
GBP4
TNF
PTGS2
GBP5
CXCL11
CCL22
RP4-620F22.2
IL1A
INHBA
aIL-10R
IL12B
CSF2
LOC541472
GBP1
IL24
aCD3aCD28 + aIL-10R
IFNG
IL6
L18MDP (3)
aIL-10R (3)
aCD3/aCD28 (4)
LPS (34)
Node size
Log2 fold change
Line width
GWAS-based and fine mapped association with IBD
d
LPS (27)
L18MDP (5)
aIL-10R (2)
aCD3/aCD28 (3)
SERPINB3
MCEMP1
ABHD17C
SLC16A10
ADAMDEC1
ITGAV
CLEC4D
SMPDL3A
CD14
LPS + aIL-10R
FAM20A
CXCL13
FABP4
SERPINB4
NLRC4
SH3PXD2B
CA12
LRP1
CD300E
S100A12
TM4SF1
TNFRSF21
DAB2
FN1
VCAN-AS1
aCD3aCD28 + aIL-10R
CD163
VCAN
MUCL1
CEMIP
L18MDP + aIL-10R

Fig. 1: Responses of PBMC from patients with IBD towards microbial stimulation and T cell activation in the context of IL-10 signalling blockade.

Microarray analysis of patients with IBD (n=41; Supplementary Table 1) PBMC samples under a variety of stimulation conditions**. (a)** The heatmap shows transcripts found to be significantly differentially expressed (columns, fold change > 1.5, BH-adjusted p-value < 0.05) in the patient samples (rows) across diverse stimulation conditions (LPS, L18MDP and αCD3/αCD28) at 16 hours post stimulation. **(b)** Venn-diagram of differentially regulated genes in the three stimulation conditions **(**LPS, L18MDP, and αCD3/αCD28 coated beads). **(c, d)** Networks of genes significantly up-regulated (**c**) or downregulated (**d**) by IL-10 signalling blockade (aIL-10R) in unstimulated (black), LPS stimulated (red), L18MDP stimulated (green) and αCD3/αCD28 stimulated (blue) patient samples (|fc| > 1.5; node size and edge-thickness are proportional to fold change).

Fig. 2

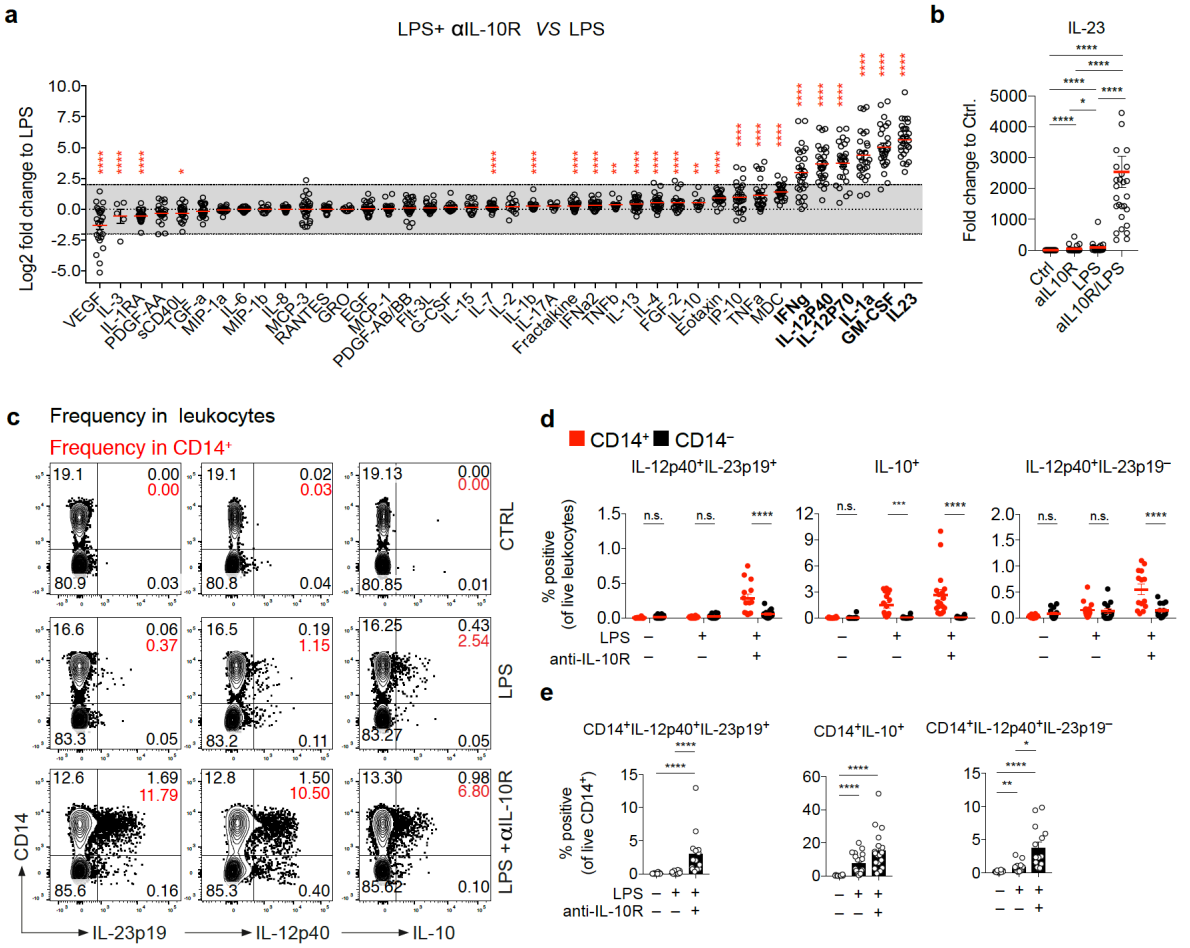
a
LPS+ αIL-10R VS LPS
Log2 fold change to LPS
VEGF
IL-3
IL-1RA
PDGF-AA
sCD40l
TGF-a
MIP-1a
IL-6
MIP-1b
IL-8
MCP-3
RANTES
GRO
EGF
MCP-1
PDGF-AB/BB
Fit-3L
G-CSF
IL-15
IL-7
IL-2
IL-1b
IL-17A
Fractalkine
IFNa2
TNFb
IL-13
IL-4
FGF-2
IL-10
Eotaxin
IP-10
TNFa
MDC
IFNg
IL-12P40
IL-12P70
IL-1a
GM-CSF
IL23
b
IL-23
Fold change to Ctrl.
Ctrl
αIL10R
LPS
αIL10R/LPS
c
Frequency in leukocytes
Frequency in CD14+
CTRL
LPS
LPS +αIL-10R
CD14
IL-23p19
IL-12p40
IL-10
d
CD14+ CD14−
IL-12p40+IL-23p19+
IL-10+
IL-12p40+IL-23p19−
% positive (of live leukocytes)
LPS
anti-IL-10R
e
CD14+IL-12p40+IL-23p19+
CD14+IL-10+
CD14+IL-12p40+IL-23p19−
% positive (of live CD14+)

Fig. 2: Monocyte-derived IL-10 regulates IL-12p40 and IL-23p19 protein synthesis and secretion in a subset of monocytes.

(a) Luminex analysis of PBMC from patients with IBD culture supernatants collected after 16 hours stimulation with LPS in presence or absence of an IL-10R blocking antibody expressed as log2 fold change to LPS stimulation (n = 28). Mean +/– SEM; Wilcoxon test, FDR-adjusted p-values. **(b)** Summary of IL-23 protein concentrations in culture supernatants following 16 hours stimulation expressed as fold change to unstimulated PBMC (n = 28). Mean +/– SEM; Friedman test, FDR-adjusted p-values. **(c)** Contour plot presentation of IL-23p19-, IL-12p40- and IL-10-producing live leukocytes and CD14 surface expression measured at 16 hours post stimulation in PBMC from patients with IBD. **(d)** Summary of frequencies of IL-12p40^{+}IL-23p19^{+}, IL-10^{+} and IL-12p40^{+}IL-23p19^{-} CD14^{+} and CD14^{-} cells as assessed by surface and intracellular staining by flow cytometry in PBMC from patients with IBD of total live leukocytes. **(e)** Summary of frequencies of IL-12p40^{+}IL-23p19^{+}, IL-10^{+} and IL-12p40^{+}IL-23p19^{-} of CD14^{+} cells (n = 18; Mean +/– SEM; Mann-Whitney test).

Fig. 3

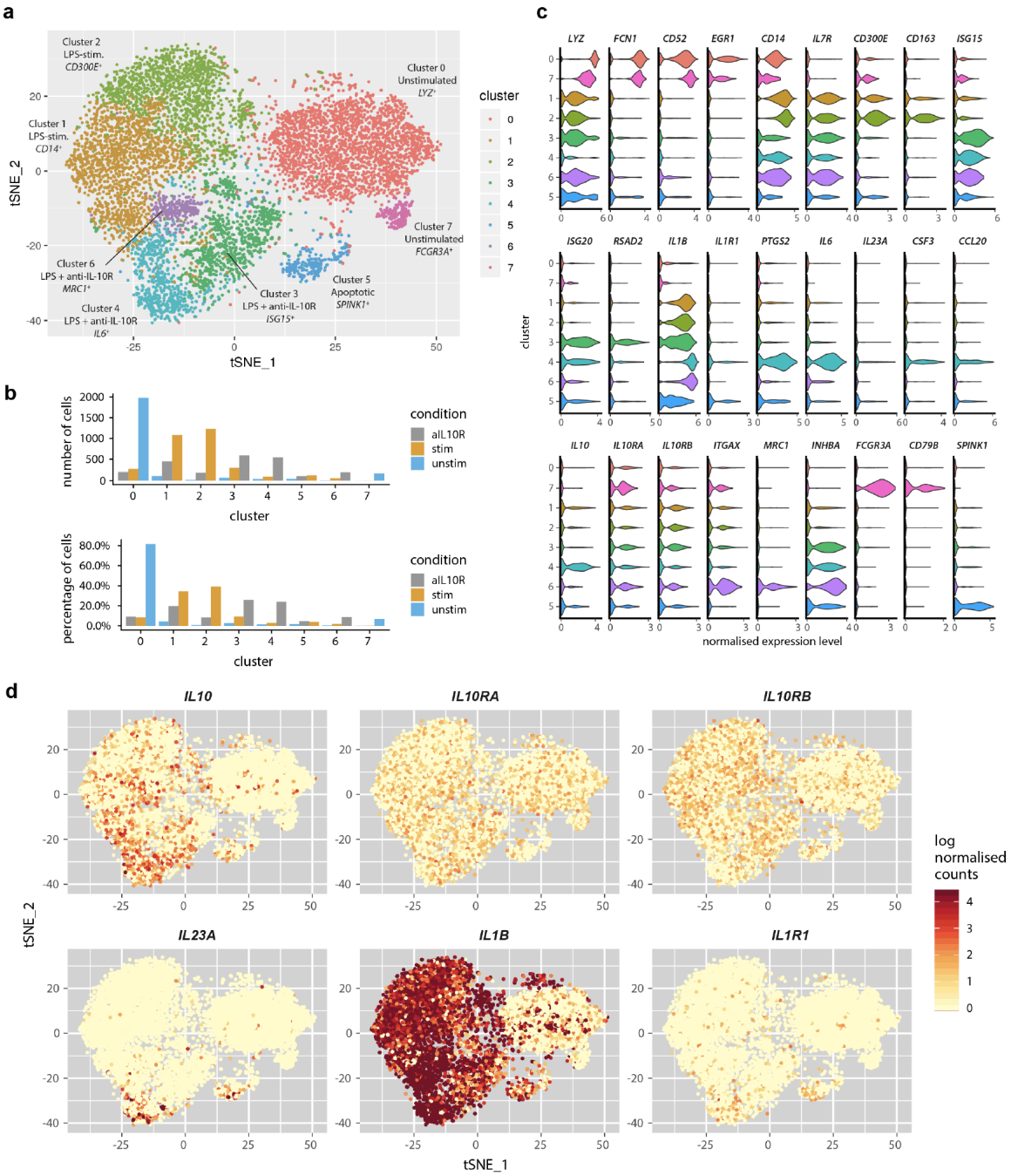
a
Cluster 2
LPS-stim.
CD300E+
Cluster 0
Unstimulated
LYZ+
Cluster 1
LPS-stim.
CD14+
Cluster 7
Unstimulated
FCGR3A+
Cluster 6
LPS + anti-IL-10R
MRC1+
Cluster 5
Apoptotic
SPINK1+
Cluster 3
LPS + anti-IL-10R
ISG15+
Cluster 4
LPS + anti-IL-10R
IL6+
tSNE_2
tSNE_1
cluster
b
number of cells
percentage of cells
condition
alL10R
stim
unstim
cluster
c
LYZ
FCN1
CD52
EGR1
CD14
IL7R
CD300E
CD163
ISG15
ISG20
RSAD2
IL1B
IL1R1
PTGS2
IL6
IL23A
CSF3
CCL20
IL10
IL10RA
IL10RB
ITGAX
MRC1
INHBA
FCGR3A
CD79B
SPINK1
normalised expression level
d
IL10
IL10RA
IL10RB
IL23A
IL1B
IL1R1
log
normalised
counts
tSNE_2
tSNE_1

Fig. 3: Single cell RNA-sequencing identifies subsets of inflammatory monocyte.
(a) The tSNE plot shows the sub-populations of unstimulated, LPS-stimulated and combined LPS and anti-IL-10R stimulated monocytes that were identified by a graph-based clustering approach following cross-condition alignment with Harmony[49] **(b)** The bar plots show the number and frequency of cells from the three stimulation conditions in each of the identified clusters. **(c)** The violin plots showing expression (x axis) of genes characteristic of the identified monocyte clusters (y-axis). **(d)** Expression of *IL10, IL10RA, IL10RB, IL23A, IL1B and IL1R1* across the single monocytes according to figure (a).

Fig. 4

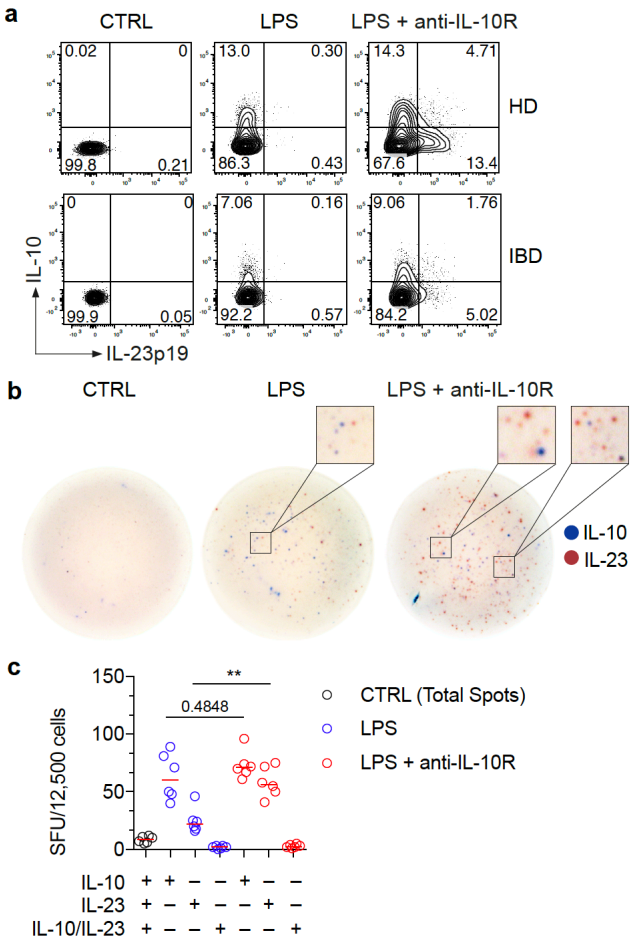
a
CTRL
LPS
LPS + anti-IL-10R
HD
IBD
IL-10
IL-23p19
0.02
0
99.8
0.21
13.0
0.30
86.3
0.43
14.3
4.71
67.6
13.4
0
0
99.9
0.05
7.06
0.16
92.2
0.57
9.06
1.76
84.2
5.02
b
CTRL
LPS
LPS + anti-IL-10R
IL-10
IL-23
c
SFU/12,500 cells
150
100
50
0
**
0.4848
CTRL (Total Spots)
LPS
LPS + anti-IL-10R
IL-10 + + – – + – –
IL-23 + – + – – + –
IL-10/IL-23 + – – + – – +

Fig. 4: The monocyte response to PRR stimulation is heterogeneous revealing a paracrine mechanism of IL-10-depedent regulation of IL-23 production.
(a) Representative contour plot presentation showing IL-23p19^{+} and IL-10^{+} frequencies in monocytes derived from a healthy donor and a patient with IBD at 16 hours post stimulation. **(b)** Representative dual-colour ELISpot images showing non-stimulated, LPS-stimulated and combined LPS and anti-IL-10R-stimulated monocytes IL-10 secretion (blue) and IL-12p40^{+}IL-23p19^{+} secretion (red). **(c)** Summary of dual-colour ELISpot measurements from 3 independent experiments (n = 6, Mean +/– SEM; Mann-Whitney test).

Fig. 5

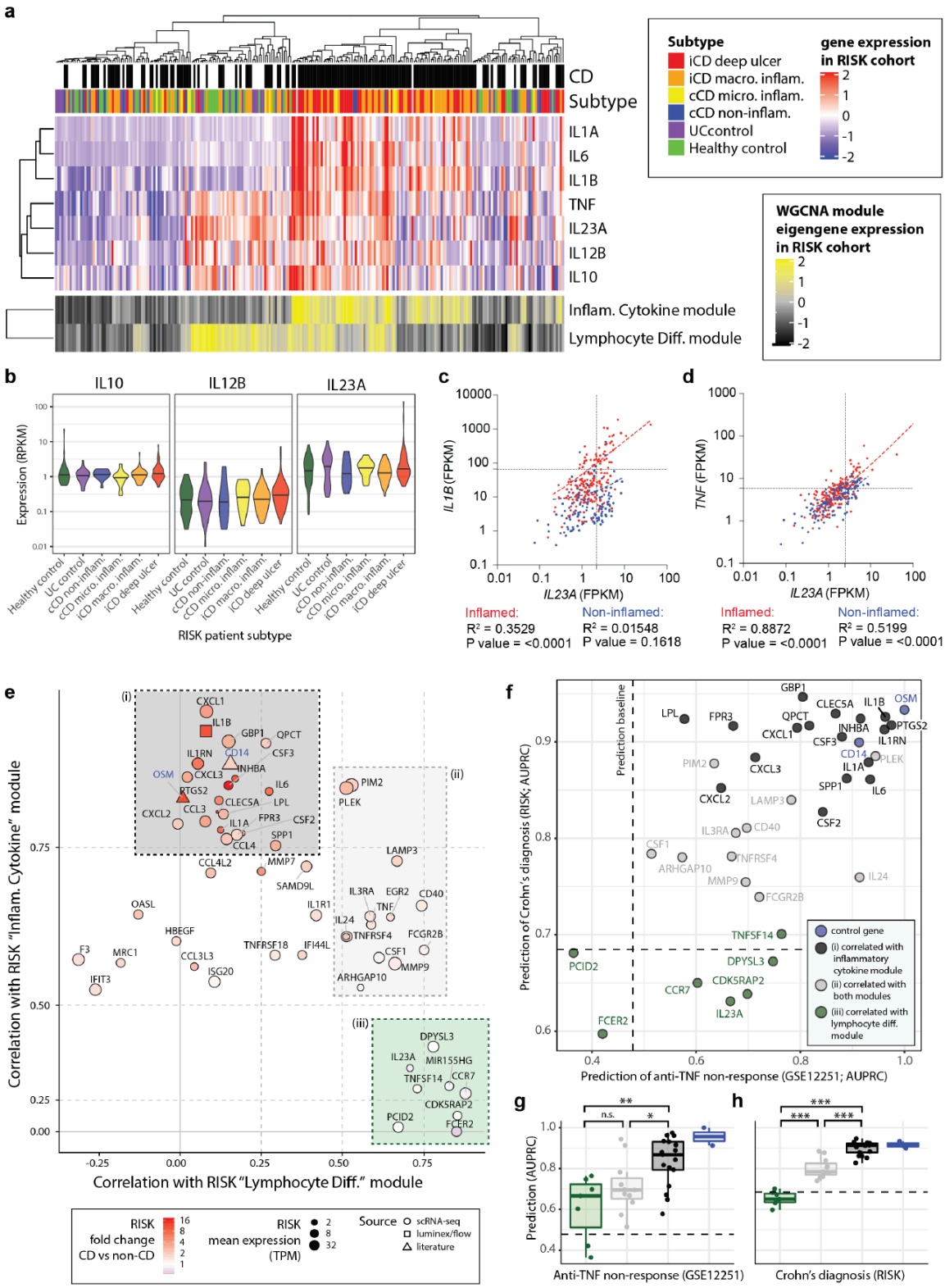
a
CD
Subtype
IL1A
IL6
IL1B
TNF
IL23A
IL12B
IL10
Inflam. Cytokine module
Lymphocyte Diff. module
Subtype
iCD deep ulcer
iCD macro. inflam.
cCD micro. inflam.
cCD non-inflam.
UCcontrol
Healthy control
gene expression in RISK cohort
WGCNA module eigengene expression in RISK cohort
b
IL10
IL12B
IL23A
Expression (RPKM)
Healthy control
UC control
cCD non-inflam.
cCD micro. inflam.
iCD macro. inflam.
iCD deep ulcer
RISK patient subtype
c
IL1B (FPKM)
IL23A (FPKM)
Inflamed:
R² = 0.3529
P value = <0.0001
Non-inflamed:
R² = 0.01548
P value = 0.1618
d
TNF (FPKM)
IL23A (FPKM)
Inflamed:
R² = 0.8872
P value = <0.0001
Non-inflamed:
R² = 0.5199
P value = <0.0001
e
Correlation with RISK "Inflam. Cytokine" module
Correlation with RISK "Lymphocyte Diff." module
(i)
(ii)
(iii)
RISK fold change CD vs non-CD
RISK mean expression (TPM)
Source
scRNA-seq
luminex/flow
literature
f
Prediction baseline
Prediction of Crohn's diagnosis (RISK; AUPRC)
Prediction of anti-TNF non-response (GSE12251; AUPRC)
control gene
(i) correlated with inflammatory cytokine module
(ii) correlated with both modules
(iii) correlated with lymphocyte diff. module
g
Prediction (AUPRC)
Anti-TNF non-response (GSE12251)
h
Crohn's diagnosis (RISK)

Fig. 5: An IL-10-regulated inflammatory monocyte gene signature informs IL-23 and IL-1 targeting therapeutic approaches in inflammatory bowel disease. (a) Patients of the paediatric RISK cohort (diagnosis and subtype as shown in top panels) were clustered according to the expression of 22 modules of co-expressed genes (see Supplementary Figure 6**a**). The upper heatmap show expression of key cytokines across the cohort. The lower panel shows expression of the eigen-genes of two of the identified modules of co-expressed genes. (**b**) The expression of *IL10*, *IL12B* and *IL23A* within the different patient strata of the RISK cohort. (**c** and **d**) Correlation of *IL23A* with *IL1B* (**c**) and *IL23A* with *TNF* in the inflamed and non-inflamed patient biopsies of the RISK cohort. (**e**) Correlation of genes specific to LPS and anti-IL-10R stimulated monocytes with the "inflammatory cytokine" and "lymphocyte differentiation" gene modules in the RISK cohort data identifies three subsets (shaded (i) black, (ii) grey and (iii) green boxes). (**f**) Assessment of the ability of the identified monocyte genes to predict anti-TNF non-response (x axis, GSE12251) and diagnosis of Crohn's (y axis, RISK cohort). The dashed lines indicate random classifier performance. (**g**) and (**h**): comparison of the ability of the identified subsets of monocyte genes to predict *TNF* non-response in the Janssen cohort and diagnosis of CD in the RISK cohort (Wilcoxon tests, colors as shown in panels (**e**) and (**f**)). AUPRC: area under precision recall curve.

Fig. 6

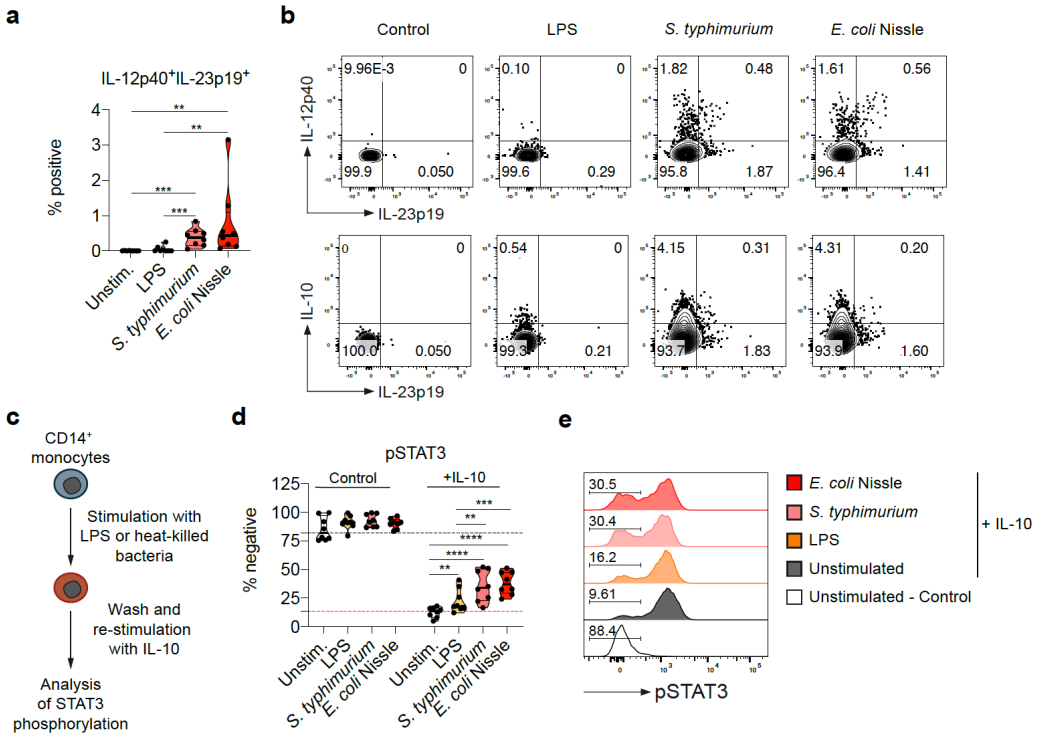
a
IL-12p40+IL-23p19+
% positive
Unstim.
LPS
S. typhimurium
E. coli Nissle
b
Control
LPS
S. typhimurium
E. coli Nissle
IL-12p40
IL-23p19
IL-10
9.96E-3
0
99.9
0.050
0.10
0
99.6
0.29
1.82
0.48
95.8
1.87
1.61
0.56
96.4
1.41
0
0
100.0
0.050
0.54
0
99.3
0.21
4.15
0.31
93.7
1.83
4.31
0.20
93.9
1.60
c
CD14+ monocytes
Stimulation with LPS or heat-killed bacteria
Wash and re-stimulation with IL-10
Analysis of STAT3 phosphorylation
d
pSTAT3
Control
+IL-10
% negative
e
30.5
30.4
16.2
9.61
88.4
pSTAT3
E. coli Nissle
S. typhimurium
LPS
Unstimulated
Unstimulated - Control
+ IL-10

Fig. 6: Monocyte uptake of whole bacteria causes IL-10 resistance and IL-23 secretion. **(a)** Summary of frequencies of IL-12p40^{+}IL-23p19^{+} live CD14^{+} cells as assessed by intracellular staining measured at 16 hours following stimulation (n=8, Mean +/– SEM; Mann-Whitney test). **(b)** Representative dot plots showing intracellular IL-12p40, IL-23p19 and IL-10 in live CD14^{+} monocytes from one healthy donor. (**c**) Experimental scheme for the assessment of monocyte IL-10 responsiveness post stimulation. (**d**) Summary of frequencies of phospho-STAT3^{-} live monocytes without cytokine stimulation (Control) and following 15 minutes IL-10 (50 ng/µl) stimulation assessed by intracellular staining (n=8, Mean +/– SEM; Mann-Whitney test). (**e**) Representative histograms showing phosphorylation of STAT3 in non-treated (Control) or IL-10 treated (+ IL-10) live monocytes. Percentages of IL-10 stimulation-resistant monocytes are indicated.

Fig. 7

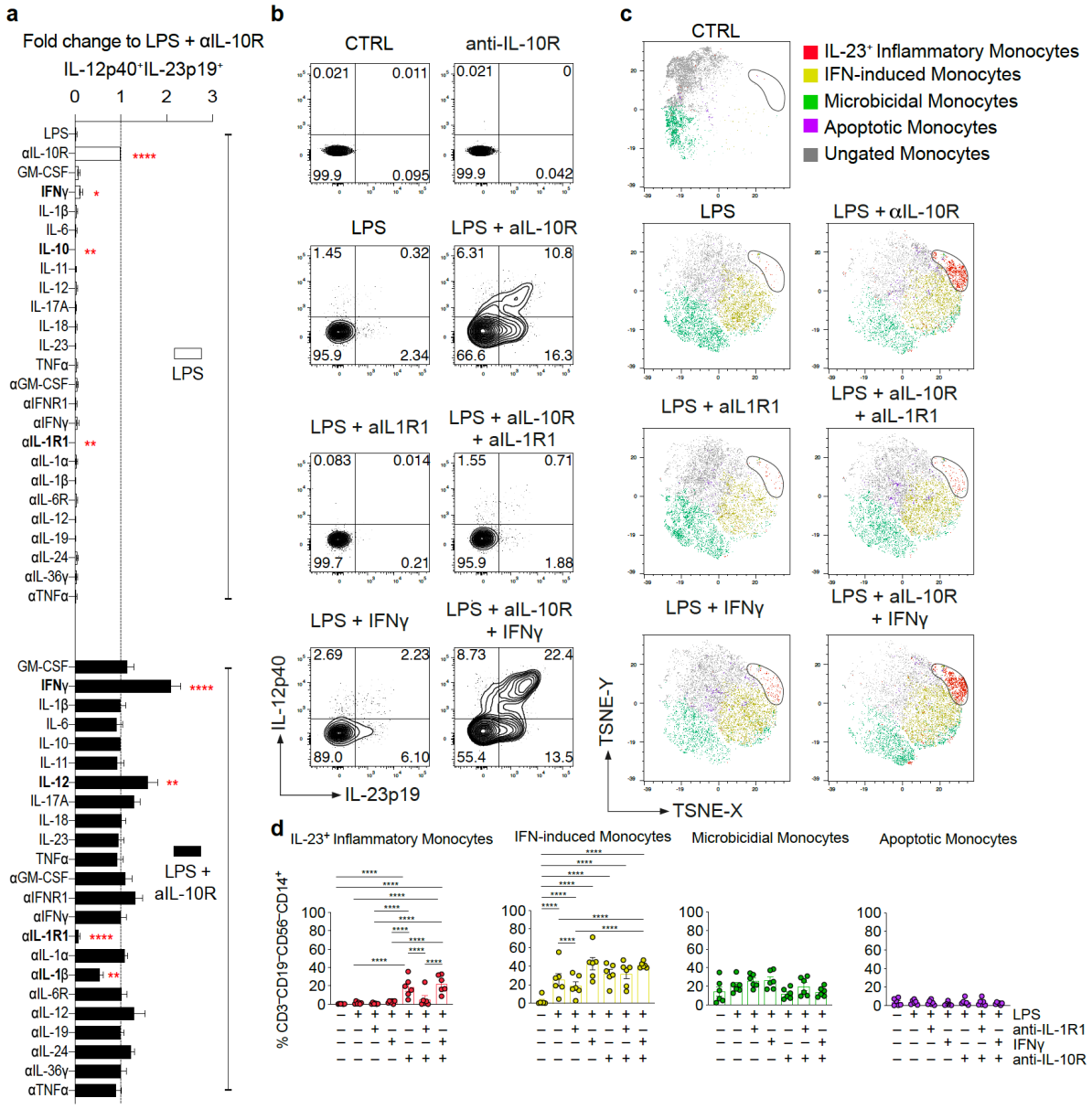
a
Fold change to LPS + αIL-10R
IL-12p40⁺IL-23p19⁺
0 1 2 3
LPS
αIL-10R
GM-CSF
IFNγ
IL-1β
IL-6
IL-10
IL-11
IL-12
IL-17A
IL-18
IL-23
TNFα
αGM-CSF
αIFNR1
αIFNγ
αIL-1R1
αIL-1α
αIL-1β
αIL-6R
αIL-12
αIL-19
αIL-24
αIL-36γ
αTNFα
LPS
LPS + αIL-10R
b
CTRL
anti-IL-10R
LPS
LPS + αIL-10R
LPS + αIL1R1
LPS + αIL-10R + αIL-1R1
LPS + IFNγ
LPS + αIL-10R + IFNγ
IL-12p40
IL-23p19
c
CTRL
IL-23⁺ Inflammatory Monocytes
IFN-induced Monocytes
Microbicidial Monocytes
Apoptotic Monocytes
Ungated Monocytes
LPS
LPS + αIL-10R
LPS + αIL1R1
LPS + αIL-10R + αIL-1R1
LPS + IFNγ
LPS + αIL-10R + IFNγ
TSNE-Y
TSNE-X
d
IL-23⁺ Inflammatory Monocytes
IFN-induced Monocytes
Microbicidial Monocytes
Apoptotic Monocytes
% CD3⁻CD19⁻CD56⁻CD14⁺
LPS
anti-IL-1R1
IFNγ
anti-IL-10R

Fig. 7: IL-1α and IL-1β signalling are essential for inducing monocyte IL-23 production. PBMC from healthy donors (n = 4-20) were stimulated for 16 hours with combinations of LPS and αIL-10R in the presence of indicated exogenous human recombinant cytokine (all 10 ng/ml), and cytokine or cytokine receptor blockade (all antibodies 10 µg/ml). **(a)** The frequencies of cytokine producing live $CD14^+$ cells were assessed by intracellular staining. Summary of IL-12p40$^+$IL-23p19$^+$ cell frequencies measured under diverse stimulation conditions (Wilcoxon test; 95% CI). **(b)** Representative dot plot showing intracellular IL-12p40 and IL-23p19 expression in $CD14^+$ monocytes of one healthy donor. **(c)** tSNE presentation of IL-23p19, CCL20, HLA-DR, IDO-1, CCL2, S100A8, RPS6 and SPINK-1 expression in live $CD14^+CD3^-CD19^-CD56^-$–gated monocytes. 3000 down-sampled monocytes from 3 healthy donors are shown as overlay. **(d)** Frequencies of monocyte clusters across stimulation conditions based on top cluster-specifying protein expression (n = 6; one way ANOVA after false discovery rate (Benjamini & Hochberg) correction).

Fig. 8

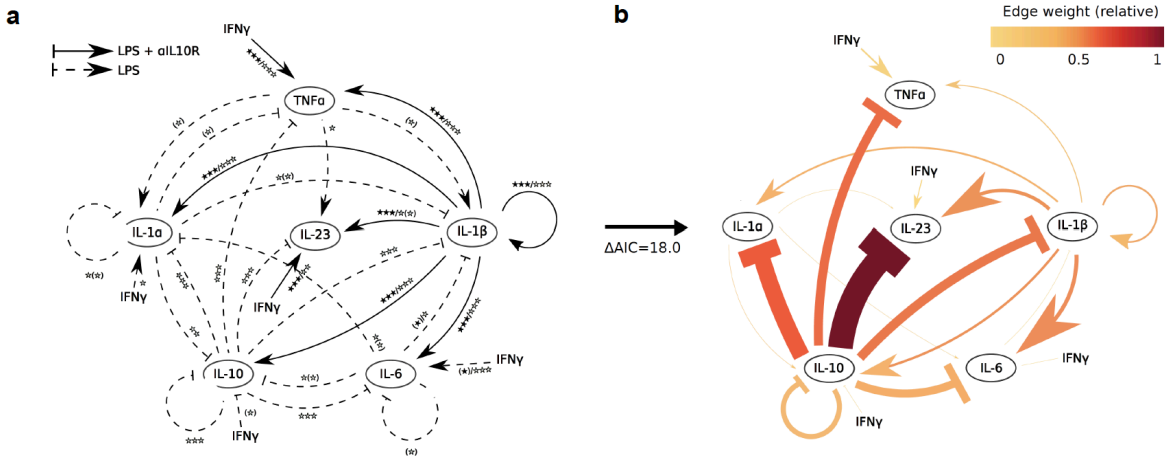
a
LPS + aIL10R
LPS
IFNγ
TNFα
IL-1α
IL-23
IL-1β
IL-10
IL-6
b
Edge weight (relative)
0
0.5
1
ΔAIC=18.0

Fig. 8: Summary of a mathematical model describing the modulation of monocyte IL-23 expression. Experimental data are based on protein expression in monocytes investigated by flow cytometry measurements of PBMC stimulated as described in Figure 6. **a)** The extensive model represents the effects of the addition or blockade of cytokines in a PBMC culture in the presence of LPS or LPS and anti-IL-10R. Cytokine responses were quantified by the frequency of cytokine (*i.e.* TNF, IL-1α, IL-1β, IL-6, IL-10 or IL-23) producing live $CD14^+$ cells multiplied by the mean fluorescence intensity within those cells. Wilcoxon test was performed to identify differences of cytokine addition or blockade in LPS stimulated samples ($^{☆}p \leq 0.05$, $^{☆☆}p \leq 0.01$, $^{☆☆☆}p \leq 0.001$; dashed arrows), in LPS and anti-IL-10R-stimulated samples ($^{★}p \leq 0.05$, $^{★★}p \leq 0.01$, $^{★★★}p \leq 0.001$; solid arrows), and in LPS and anti-IL-10R-stimulated and anti-IL-1β treated conditions (dotted arrows). Nominal effects with $p>0.05$ after false discovery rate (Benjamini & Hochberg) correction are shown in parenthesis. **(b)** A reduced complexity model was established by focusing on informative cytokine interactions. The expression of the cytokines TNF, IL-1α, IL-1β, IL-6, IL-10 and IL-23 over time was described by a system of coupled ordinary differential equations. Starting from no interactions, edges were added iteratively while maximizing the increase in model fit. Edge widths are relative to the increase in fit obtained after edge addition. The Akaike information criteria (AIC) identifies the model including twenty edges as the optimal balance between model complexity and model fit. Edge weights are defined as the relative contribution to model fit and are dependent on the network configuration considered. The edges of the twenty-edge model have been coloured based on their weight.

Supplementary Fig. 1

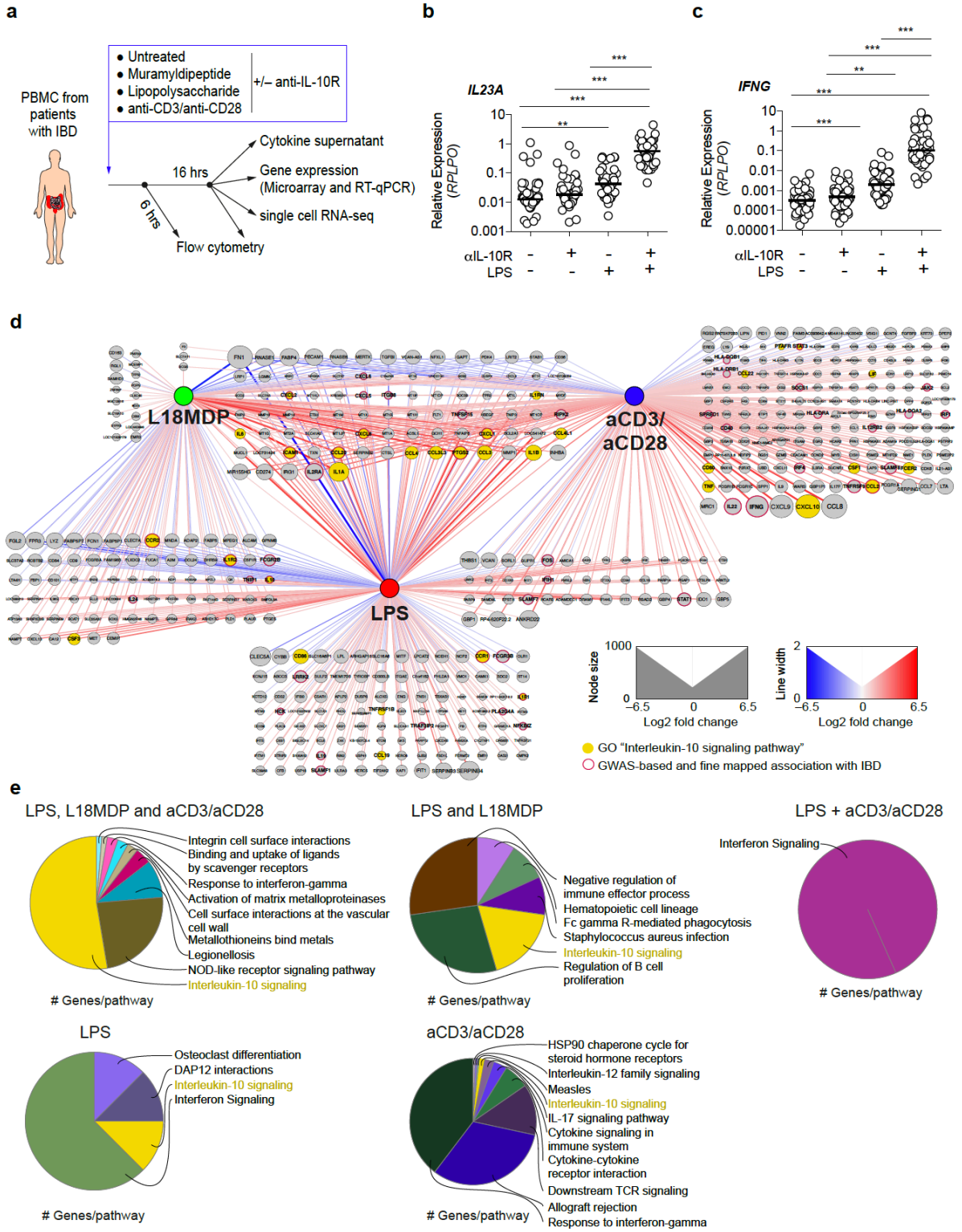

Supplementary. Fig. 1: (a) Graphical illustration of *ex vivo* PBMC stimulations and experimental conditions. **(b, c)** RT-qPCR analysis of *IL23A* (b) and *IFNG* (c) gene expression in IBD patients following 16 hours stimulation with combinations of LPS and anti-IL-10R antibody (n=45; Kurskal Wallis test). **(d)** Network analysis of stimulation regulated genes showing individual and overlapping genes regulated through LPS, L18MDP and anti-CD3/anti-CD28 stimulation. The strength of regulations of target genes is indicated through continuous mapping of the edge weight and node size based on log2 fold change values. Up- and downregulated genes are indicated as blue and red edges respectively. **(e)** Cytoscape-ClueGO pathways enrichment analysis (adjusted (Benjamini & Hochberg) $p<0.05$) of stimulation-specific and shared genes based on combined KEGG-pathways, Reactome pathways and EMBL-EBI Quick-GO pathways. The contribution of IL-10 signalling is highlighted.

Supplementary Fig. 2

a IL-10 blockade upregulated pathways:

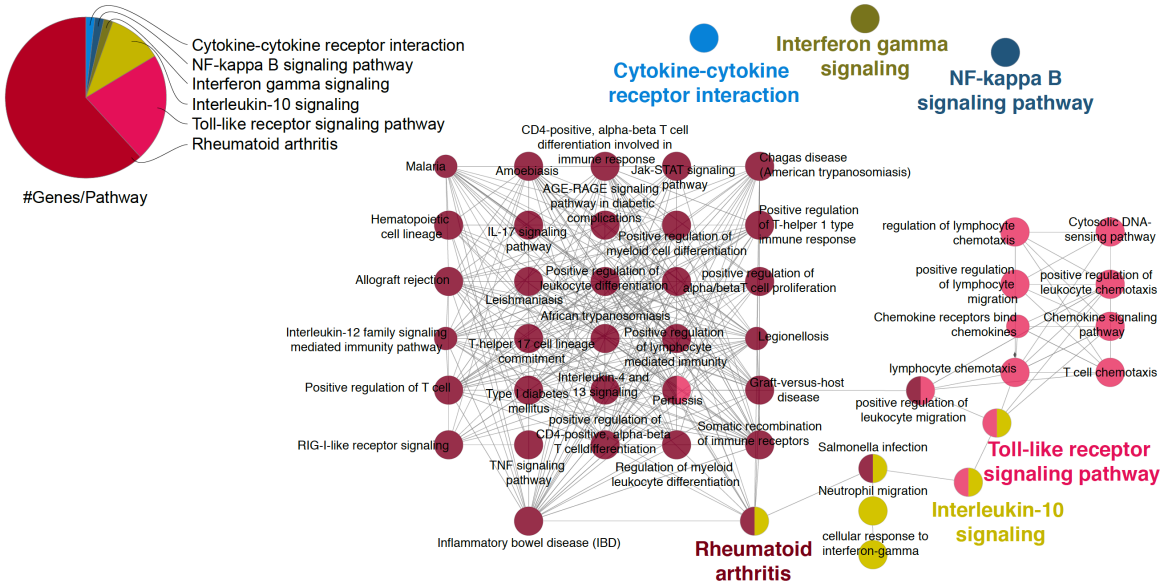

b IL-10 blockade downregulated pathways:

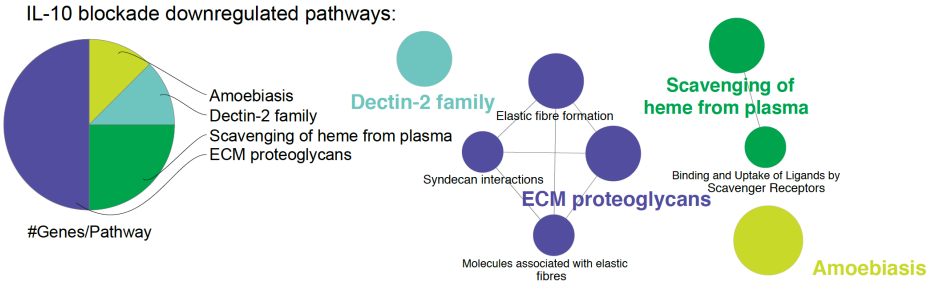

c

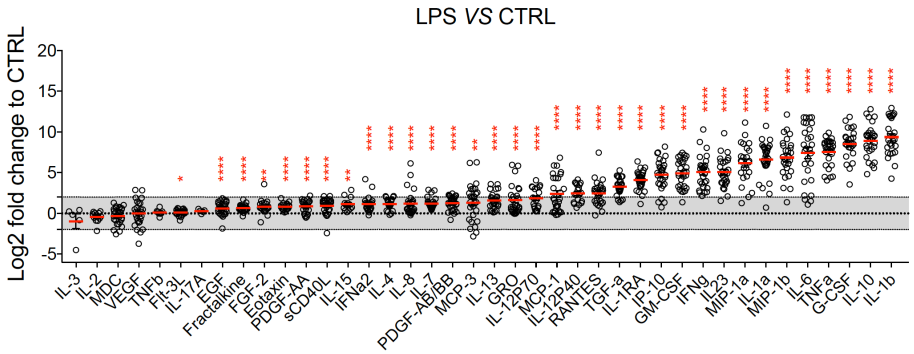

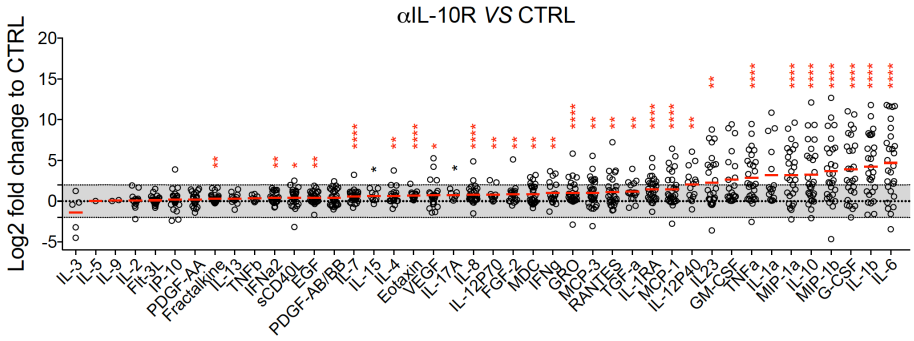

Supplementary Fig. 2: (a, b) Cytoscape-ClueGO analysis of combined EMBL-EBI QuickGO, KEGG and Reactome pathways (adjusted (Benjamini & Hochberg) p-value<0.05) associated with LPS stimulation and IL-10R blockade induced (a) and suppressed (b) genes **(c)** Luminex analysis of PBMC culture supernatants collected after 16 hours stimulation with LPS (200 ng/ml) or IL-10R blocking antibody (10 µg/ml) expressed as log2 fold change to non-stimulated PBMC supernatants (CTRL); n = 28. Mean +/– SEM; Wilcoxon test, FDR-adjusted (Benjamini & Hochberg) p-values.

Supplementary Fig. 3

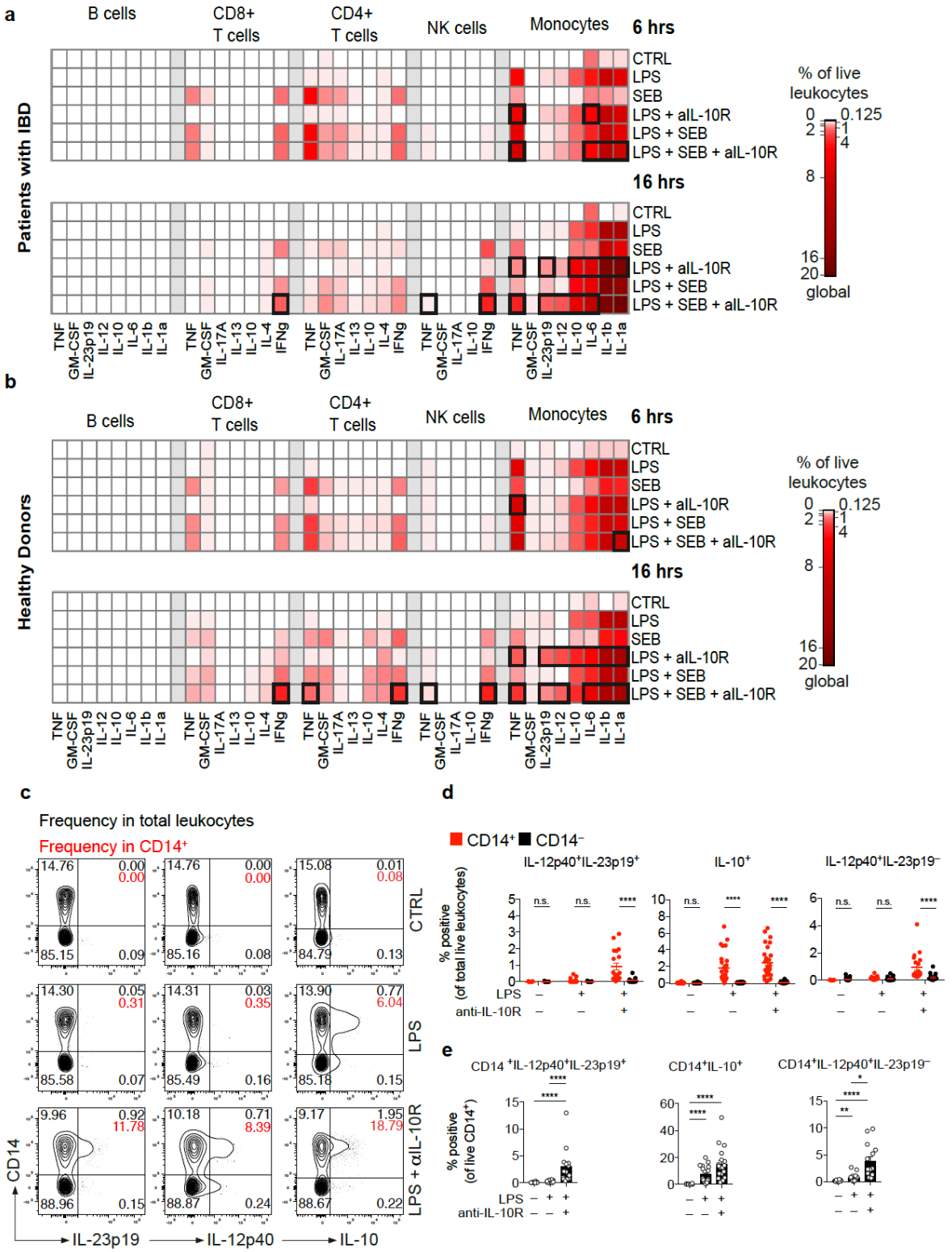

Supplementary Fig. 3: (a and b) Dot plot presentation of IL-23p19-, IL-12p40-and IL-10-producing live leukocytes and CD14 surface expression measured at 16 hours post stimulation in PBMC from patients with IBD (a) and PBMC from healthy donors (b). **(c)** Summary of frequencies of IL-12p40^{+}IL-23p19^{+}, IL-10^{+} and IL-12p40^{+}IL-23p19^{-} in CD14^{+} and CD14^{-} cells as assessed by intracellular staining and flow cytometry in PBMC from healthy individuals (n=26; Mean +/– SEM; Mann-Whitney test). **(d, e)** PBMC from patients with IBD (d; n=7) or health individuals (e; n=10) were stimulated for 6 or 16 hours with combinations of LPS (200 ng/ml), SEB (1 μg/ml) and IL-10R blocking antibodies (10 μg/ml) with BFA present for the last 4 hrs of culture. Cells were then surface stained to identify distinct leukocyte populations followed by intracellular cytokine staining. The frequency of cytokine producing cells for each population was assessed and presented as % cytokine producing cells of total live leukocytes. Monocytes were identified as CD14^{+}CD3^{-}CD19^{-}CD56^{-}, CD4^{+} T cells as CD3^{+}CD4^{+}CD8^{-}CD14^{-}CD19^{-}CD56^{-}, CD8^{+} T cells as CD3^{+}CD8^{+}CD4^{-}CD14^{-}CD19^{-}CD56^{-} NK cells as CD56^{+}CD3^{-}CD14^{-}CD19^{-} and B cells were identified as CD19^{+}CD3^{-}CD14^{-}CD56^{-} (Mean; bold squares indicate $p<0.05$; Mann-Whitney test).

Supplementary Fig. 4

a

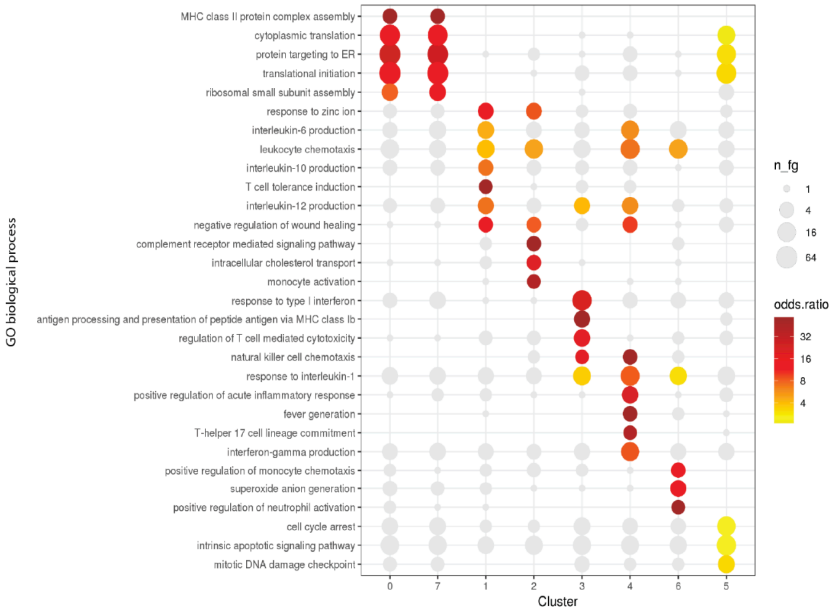

b

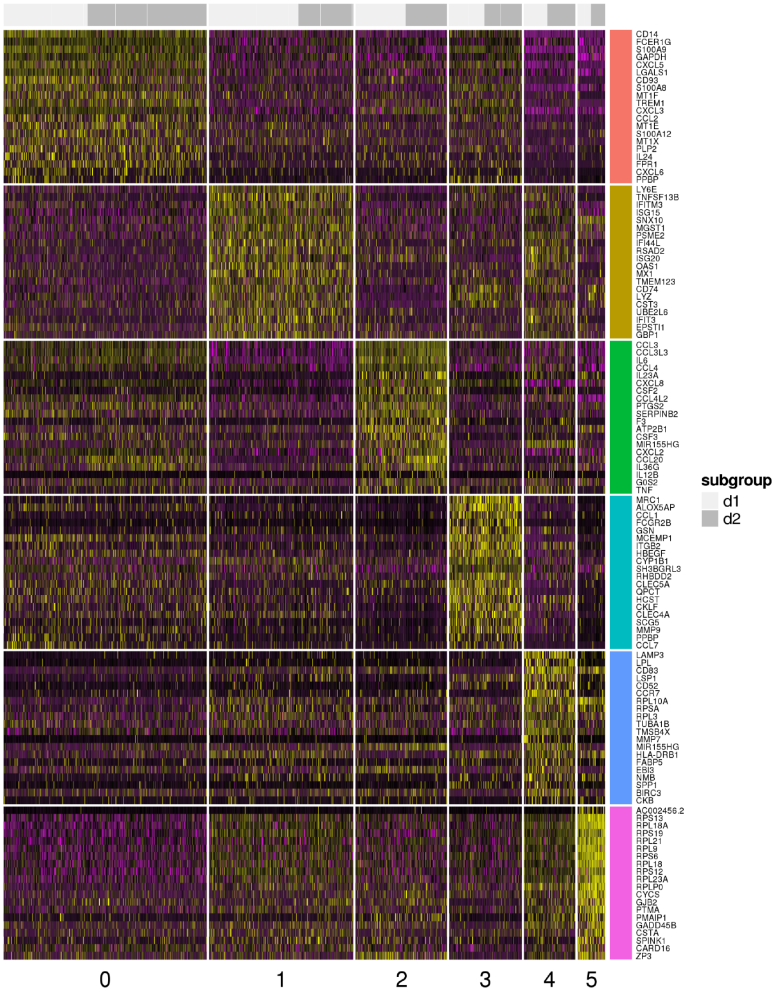

Supplementary Fig. 4: Single cell genomics identifies transcriptionally distinct monocyte clusters following combined LPS + anti-IL-10R stimulation. (a) Selected over-represented GO biological process gene sets of the 8 identified monocyte clusters across stimulation conditions (Unstimulated, LPS-stimulated and LPS + anti-IL-10R-stimulated). **(b)** Heatmap of cluster marker genes for cell-cycle corrected analysis of the LPS + anti-IL-10R condition alone (donors 1 and 2). Cluster 1 corresponds to cluster 3 in the aligned analysis (Interferon-induced monocytes), cluster 2 to cluster 4 in the aligned analysis (IL-23^{+} inflammatory monocytes) and cluster 3 to cluster 6 in the aligned analysis (MRC1^{+} microbicidial monocyte subpopulations).

Supplementary Fig. 5

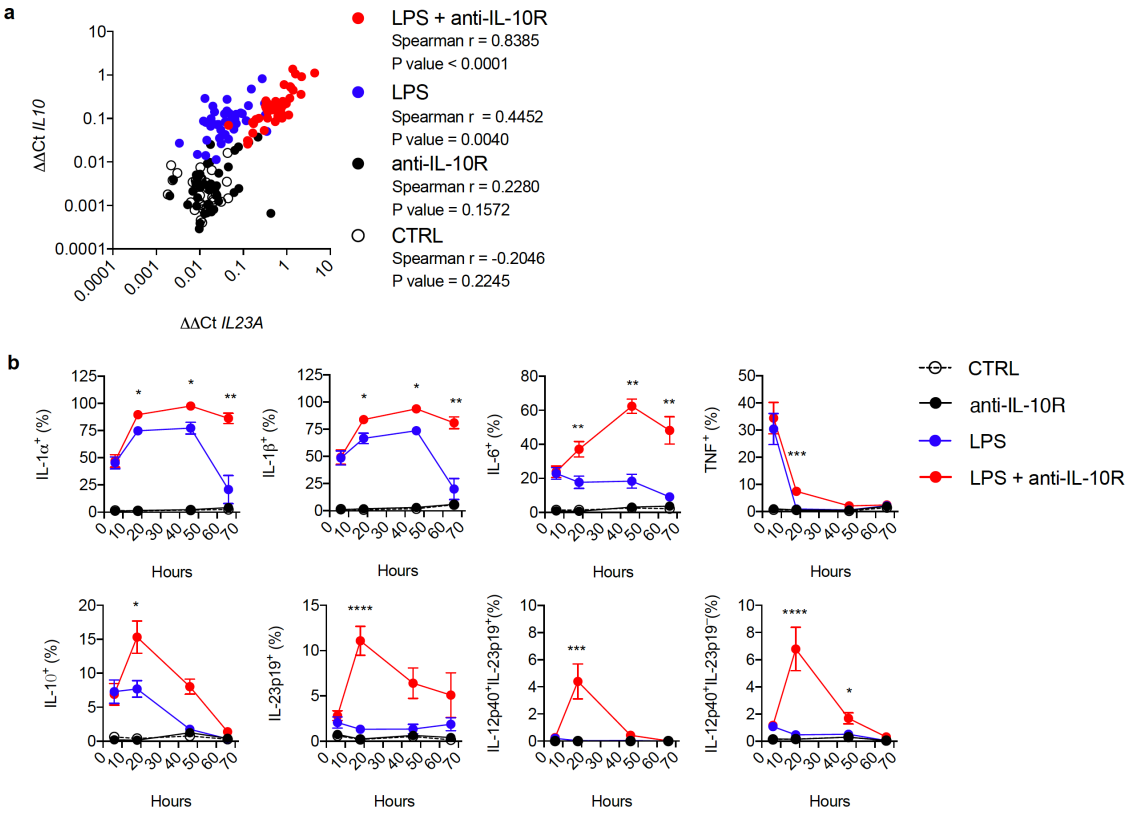

Supplementary Fig. 5: *IL23A* and *IL10* gene expression positively correlate under settings of LPS stimulation and IL-10 signalling blockade and monocytes produce cytokines with distinct kinetics. (a) RT-qPCR based ΔΔCt correlation analysis of *IL10* and *IL23A* gene expression in unstimulated, anti-IL-10R (10 μg/ml), LPS (200 ng/ml), and combined LPS and anti-IL-10R-stimulated PBMC (n=40)**. (b)** PBMC were stimulated for up to 66 hours with combinations of LPS and anti-IL-10R. The frequencies of cytokine producing live $CD14^+$ cells were assessed by surface and intracellular staining at different time points, as indicated (n=4-10, Mean +/– SEM; Kruskal-Wallis test; FDR-adjusted (Benjamini & Hochberg) p-values).

Supplementary Fig. 6

a

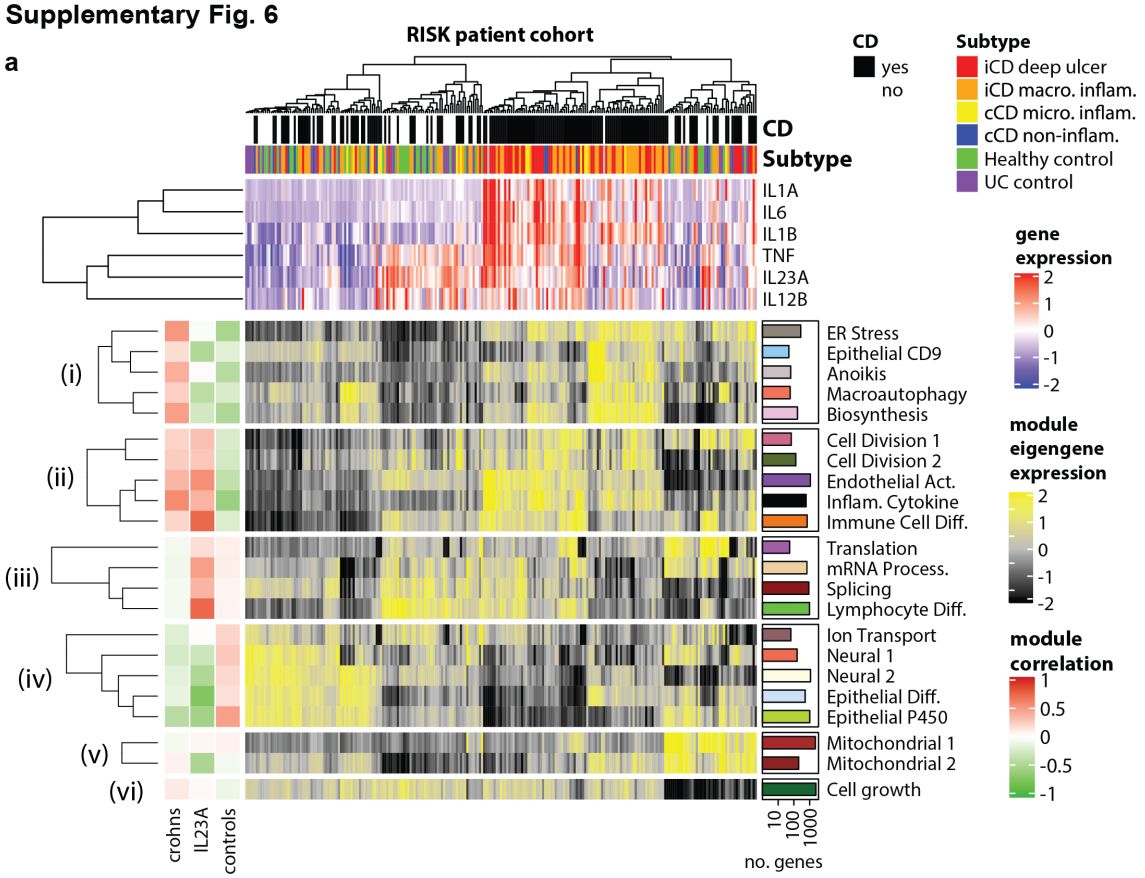

b

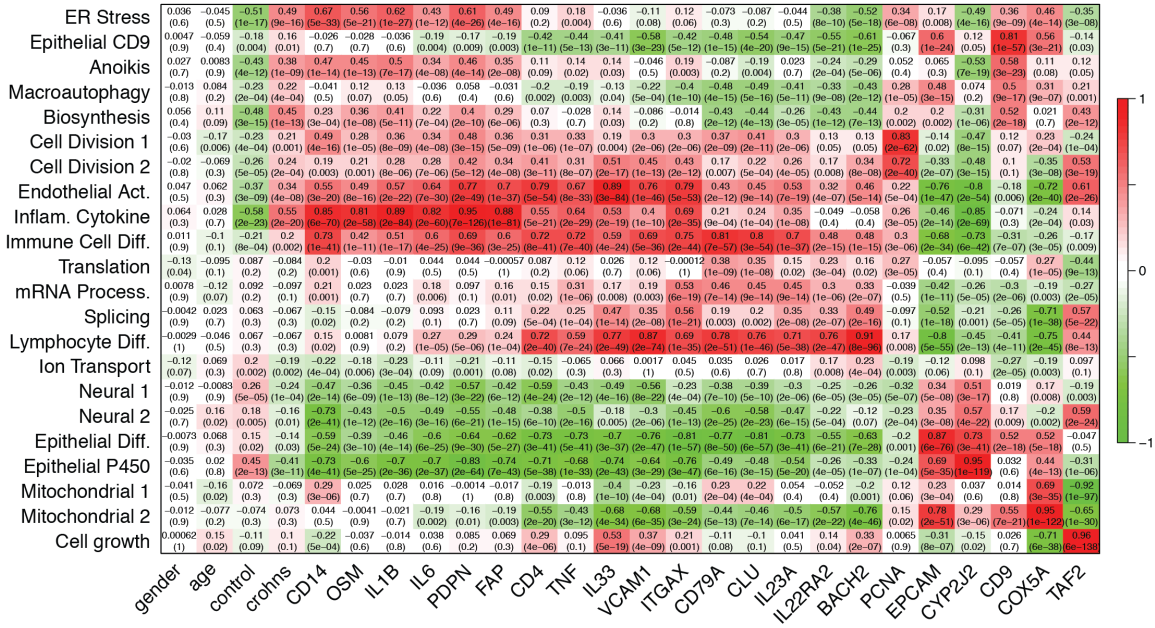

Supplementary Fig. 6: Identification of modules of co-expressed genes in patient biopsies from the paediatric RISK cohort. (a) The main heatmap shows expression of the eigen-genes of the n=22 identified modules of genes. Patients (columns) are hierarchically clustered by expression of the module eigen-genes. The heat map is annotated with (i) patient diagnosis and disease subtype (top panels), (ii) expression of key cytokines (upper heatmap), (iii) correlation of the eigen-genes with diagnosis of Crohn's disease, *IL23A* expression and control status (left panel) and (iv) the numbers of genes within each of the modules (right panel). Modules were named according to enrichments for gene ontology and cell type genesets (Supplementary Table 4). **(b)** The heatmap shows the correlation of the RISK WGCNA modules (y axis) with genes and traits of interest (x axis).

Supplementary Fig. 7

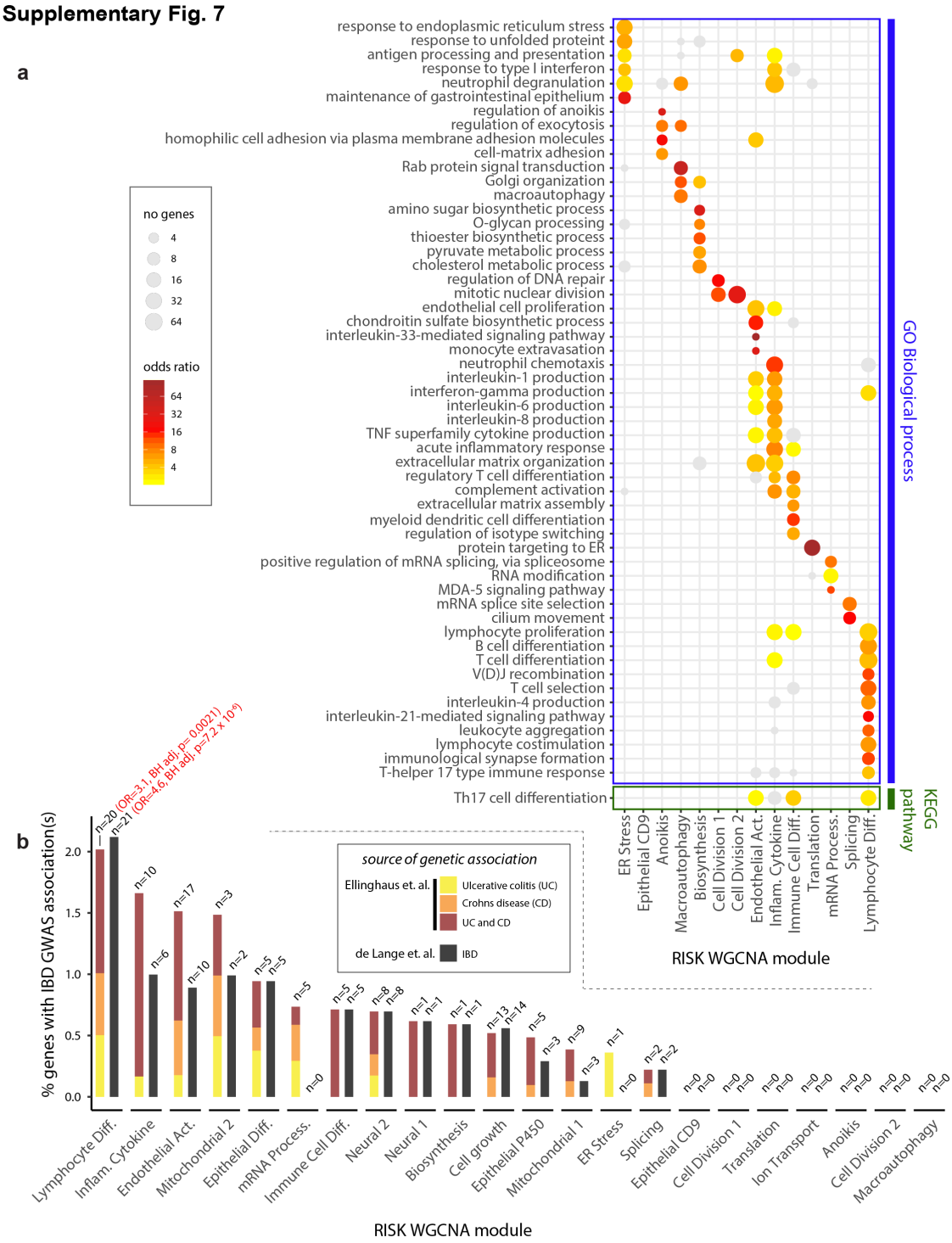

Supplementary Fig. 7: Characterisation of the RISK WGCNA modules. (**a**) The dot-plot shows the enrichment of selected biological process gene ontology categories and KEGG pathways in the WGCNA modules that were correlated with diagnosis of Crohn's disease and/or *IL23A* expression (one-sided Fisher tests, (Benjamini & Hochberg) adjusted $p<0.05$, p-values adjusted separately for GO categories and KEGG pathways). (**b**) The frequency (y axis) of IBD GWAS-associated genes in the different RISK WGCNA modules (x axis). Genetically associated genes were sourced from Ellinghaus *et. al.*[12] or de Lange *et. al.*[13] (see methods). (Benjamini & Hochberg) adjusted p-values and odds ratios are given for significant enrichments (red text).

Supplementary Fig. 8

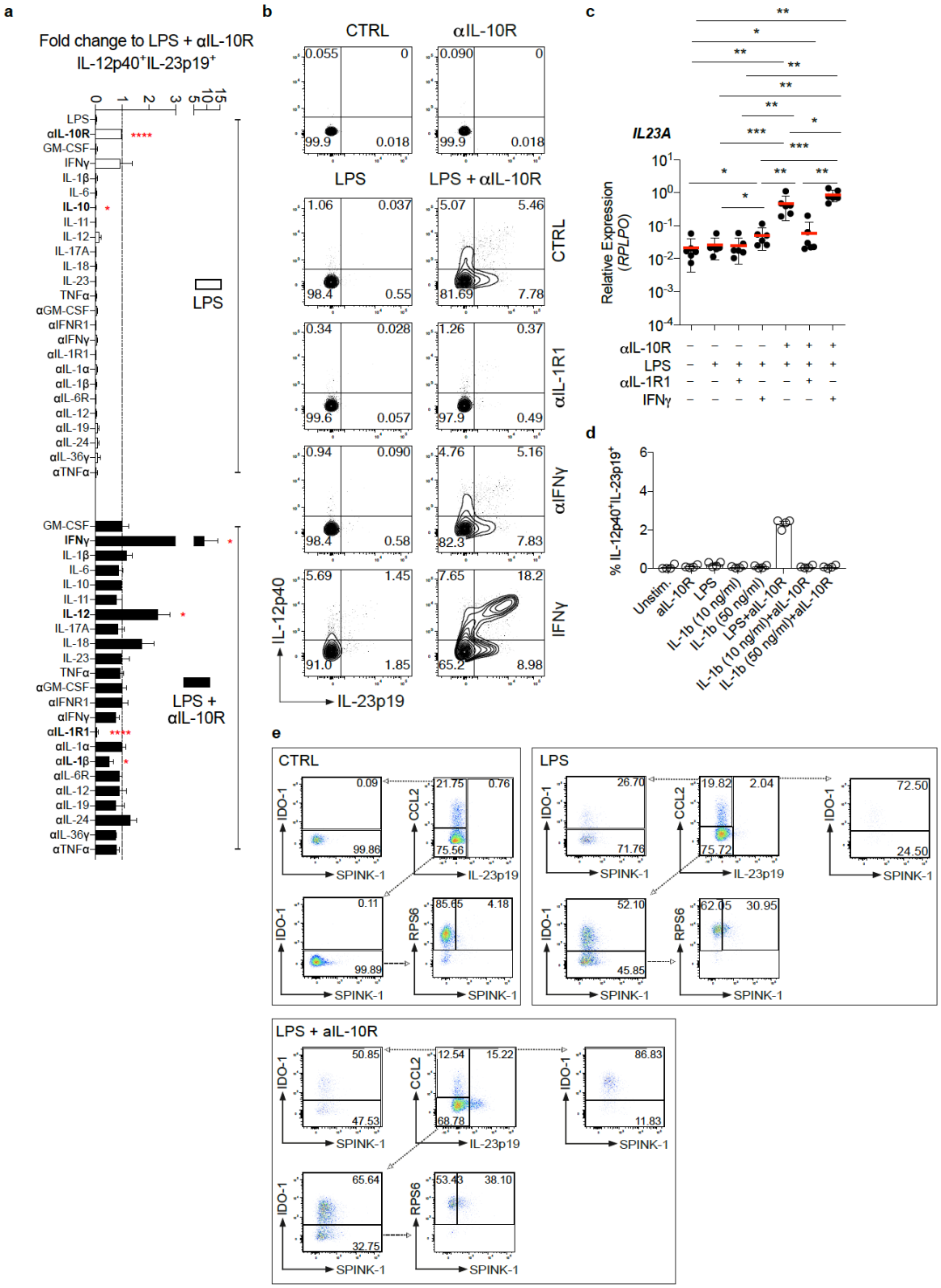

Supplementary Fig. 8: IL-1α and IL-1β signalling are essential for inducing monocyte IL-23 production. PBMC from patients with IBD (n > 4) were stimulated for 16 hours with combinations of LPS and αIL-10R in the presence of indicated exogenous human recombinant cytokine, cytokine receptor blockade or cytokine blockade. **(a)** The frequencies of cytokine producing live $CD14^+$ cells were assessed by intracellular staining. Summary of IL-$12p40^+$IL-$23p19^+$ cell frequencies measured under diverse stimulation conditions; Wilcoxon test; 95% CI). **(b)** Representative dot plot showing intracellular IL-12p40 and IL-23p19 in $CD14^+$ monocytes of one healthy donor. **(c)** RT-qPCR analysis of healthy donor PBMC stimulated with combinations of LPS, anti-IL-10R, anti-IL-1R1 and IFN-γ for 16 hours. **(d)** Frequencies of IL-$12p40^+$IL-$23p19^+$ live $CD14^+$ monocytes after 16 hours stimulation with combinations of LPS (200 ng/ml), anti-IL-10R (10 μg/ml) and IL-1β (10 and 50 ng/ml). **(e)** Dot plot presentation of one representative experiment showing live $CD14^+$-gated monocytes and sub-gating strategies based on the expression of IL-23p19, CCL2, IDO-1 RPS6 and SPINK-1 in non-stimulated, LPS-stimulated and combined LPS and anti-IL-10R stimulated PBMC.

Supplementary Fig.9

a

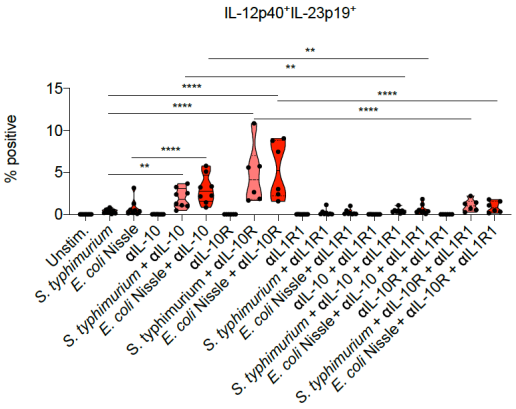

b

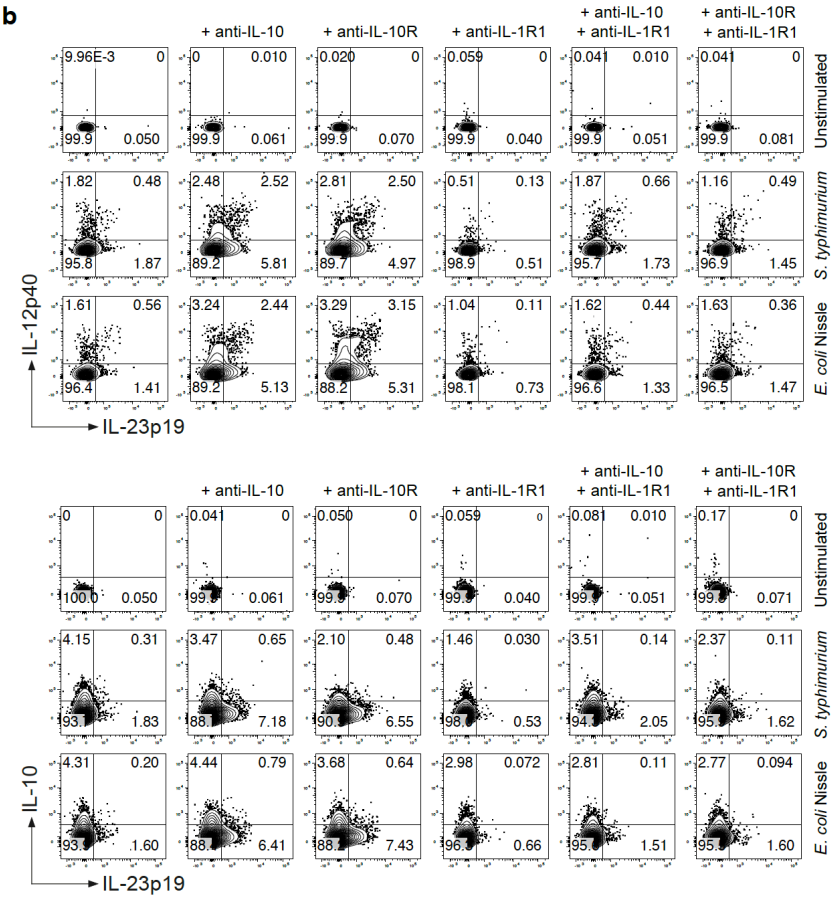

Supplementary Fig. 9: Monocyte IL-23 production induced by uptake of whole bacteria is dependent on IL-1R1 signalling. (a) Summary of frequencies of IL-12p40^{+}IL-23p19^{+} live CD14^{+} cells as assessed by intracellular staining measured in indicated conditions at 16 hours following stimulation (n=8, Mean +/– SEM; Kruskal-Wallis test; FDR-adjusted (Benjamini & Hochberg) p-values). **(b)** Representative dot plots showing intracellular IL-12p40, IL-23p19 and IL-10 in live CD14^{+} monocytes of one healthy donor.

Supplementary Fig. 10

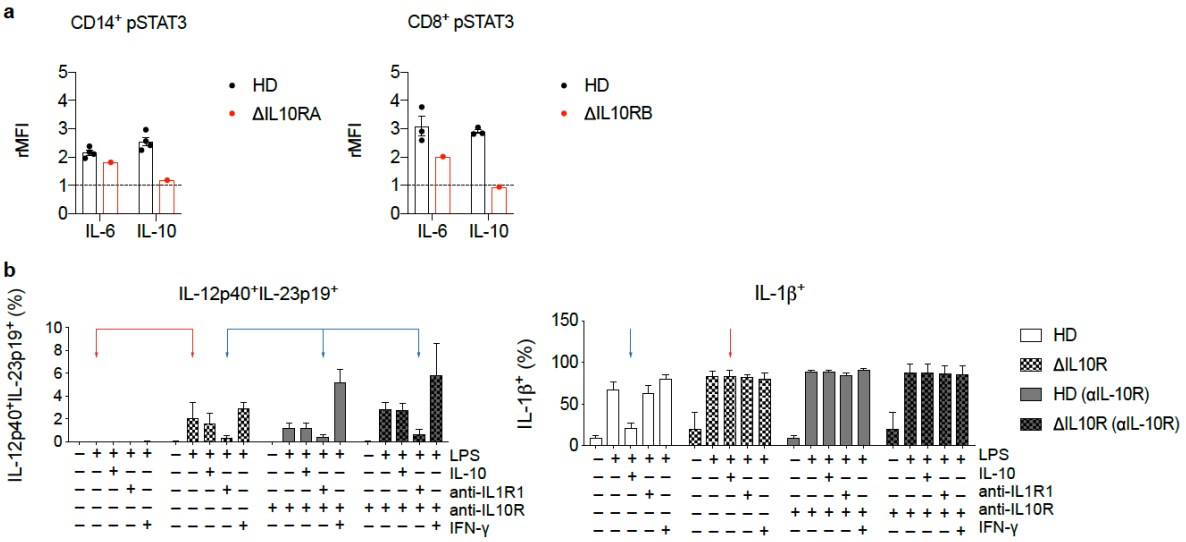

Supplementary Fig. 10: Monocyte IL-23 responses in patients with LOF in IL-10R1 and IL-10R2 are responsive to blockade of IL-1R1 signalling. (a) Analysis of STAT3 phosphorylation following recombinant human IL-6 or IL-10 stimulation in a patient with very early onset IBD carrying a loss of function variant in the gene coding for *IL10RA* (p.Y167C, left) and a patient with very early onset IBD carrying a loss of function variant in the gene coding for *IL10RB* (p.R117H, right). **(b)** Analysis of frequencies of IL-12p40^{+}IL-23p19^{+} and IL-1β^{+} monocytes following 16 hours stimulation in PBMC from healthy donors and patients with IL-10R variants with combinations of LPS (200 ng/ml), IL-10 (10 ng/ml), anti-IL-10R (10 μg/ml), anti-IL-1R1(10 μg/ml) and IFN-γ (10 ng/ml).

Material and Methods

Patient cohort - Oxford IBD cohort and Oxford Gastrointestinal biobank.

The Oxford IBD cohort study is an observational prospective cohort study that aims to understand disease susceptibility factors and outcome of patients with IBD. This study was approved by the Research Ethics Committee Reference: 09/H1204/30. Healthy donors were recruited via the Oxford gastrointestinal biobank (11/YH/0020 and 16/YH/0247). All patients with IBD and healthy volunteers provided written informed consent.

Patient cohort - RISK cohort and outcome classification.

The RISK study is an observational prospective cohort study with the aim to identify risk factors that predict complicated course in pediatric patients with Crohn's disease[1]. The RISK study recruited treatment-naive patients with a suspected diagnosis of Crohn's disease. The Paris modification of the Montreal classification were used to classify patients according to disease behaviour (non-complicated B1 disease (non-stricturing, non-penetrating disease); complicated disease, composed of B2 (stricturing) and/or B3 (penetrating) behaviour) as well as disease location (L1, ileal only, L2, colonic only, L3, ileocolonic and L4, upper gastrointestinal tract). 322 samples were investigated with ileal RNA-seq. Individuals without ileal inflammation were classified as non-IBD controls. Patients with Crohn's disease were followed over a period of 3 years. Patients were largely of European (85.7%) and African (4.1%) ancestry.

Cell isolation, culture and stimulation.

Whole blood was collected into EDTA-containing tubes. PBMC were purified using Ficoll-Paque density gradient purification. The absolute number of cells was determined using a haemocytometer (Marienfeld). For stimulation assays, $0.5x10^6$ -$1x10^6$ PBMC or MACS-

purified $CD14^+$ monocytes (Mitenyi Biotec) were cultured in 200 µl medium in duplicates in round bottom 96-well plates and exposed to ultrapure 200 ng/ml LPS (Enzo Life Sciences; Cat.# ALX-581-008), 200 ng/ml L18MDP (Invivogen) 10 µg/ml anti-IL-10R (Biolegend; clone: 3F9), anti-CD3/anti-CD28 beads (Invitrogen) or Staphylococcal enterotoxin B (SEB; Sigma) for the indicated time in complete RPMI with L-glutamine (Sigma) supplemented with 10 % human serum (Sigma; Cat.# H4522), non-essential amino acids (Gibco); 1 mM Sodium-Pyruvate (Gibco) and 100 U/ml penicillin and 10 µg/ml streptomycin (Sigma). Supernatants were collected and stored at -80 °C for the quantification of cytokine production. The following neutralizing antibodies or receptor blocking antibodies were used (all 10 µg/ml): anti-IL-24 (R&D; Cat.# AF1965; Polyclonal Goat IgG), anti-IL-12p70 (R&D; Cat.# MAB219; clone 24910), anti-IL-19 (R&D; Cat.# MAB10351; clone 152107), anti-GM-CSF (R&D; Cat.# MAB215; clone 3209), anti-IL-1R1 (R&D; Cat.# AF269; polyclonal Goat IgG), anti-IL-1α/IL-1F1 (R&D; Cat.# AF-200-NA; polyclonal Goat IgG), anti-IL-1β/IL-1F2 (R&D; Cat.# MAB201; clone: 8516), anti-IL-6R (Tocilizumab, Actemra®, Roche,), anti-TNFα (Infliximab, REMICADE®, Janssen), anti-IFNα/βR2 (Millipore; Cat.# MAB1155; clone: MMHAR-2), anti-IL-10R (Biolegend; Cat.# 308807; clone: 3F9), anti-IL-10 (R&D; Cat.# MAB217; clone: 23738), anti-IFNγ (Biolegend; Cat.# 506513; clone: B27), anti-IL-36γ (R&D; Cat.# MAB2320; clone: 278706). The following recombinant human cytokines were used (all 10 ng/ml): IL-1β (Preprotech), IL-6 (Preprotech), IL-10 (Preprotech), IL-11 (R&D), IL-12 (Preprotech), IL-17A (Preprotech), IL-18 (R&D), IL-23 (Preprotech), GM-CSF (Preprotech), IFNγ (Preprotech), TNFα (Preprotech).

Whole bacteria preparation and stimulation.

Both *Salmonella enterica serovar Typhimurium* (ST) expressing green-fluorescent protein (GFP) (NCTC 12023)[2] and *Escherichia coli* Nissle 1917[3] (EcN) were grown overnight in LB

(Sigma) and the O.D was measured on the following day at 650nm. Aliquots corresponding to 10^9 particles of bacterial were centrifuged at 6000 rpm for 5 minutes and the pellet was washed twice in the fresh LB then twice in PBS (Sigma). Cells were then heat-killed at 65°C for 30 minutes and stored in aliquots at -20°C till further use. For monocyte stimulation assays, $0.1x10^6$ MACS-purified $CD14^+$ monocytes (Mitenyi Biotec) were cultured in 150 µl medium in duplicates in round bottom 96-well plates and exposed to combinations of ST (monocyte to bacteria ratio = 1:2), EcN (monocyte to bacteria ratio = 1:2), ultrapure 200 ng/ml LPS (Enzo Life Sciences; Cat.# ALX-581-008), 10 µg/ml anti-IL-10R (Biolegend; clone: 3F9), 10 µg/ml anti-IL-10 (R&D; Cat.# MAB217; clone: 23738), 10 µg/ml anti-IL-1R1 (R&D; Cat.# AF269; polyclonal Goat IgG) for 16 hours (the last 4 hours of culture in the presence of BFA (Sigma) in the case of intracellular staining) in complete RPMI with L-glutamine (Sigma) supplemented with 10 % human serum (Sigma; Cat.H4522), non-essential amino acids (Gibco); 1 mM Sodium-Pyruvate (Gibco) and 100 U/ml penicillin and 10 µg/ml streptomycin (Sigma).

Protein level analysis.

Cytokine levels in the supernatants were assayed using the Milliplex human cytokine/chemokine magnetic bead 41-plex panel (Milliplex Billerica, MA, USA; HCYTOMAG-60K-PX41) and acquired on a Luminex LX200 flow reader. IL-23p19 cytokine level was assayed using a MSD (Meso Scale Discovery) in-house assay. In short, an IL-23p-19 selective antibody (Ab1, clone #32) was biotinylated following the Biotin, EZ-Link™ NHS-PEG4-Biotin instructions (ThemoScientific, Cat.# 2161299). For detection, an anti-p40 antibody (Ab-2, clone #42) was sulfotaged according to manufactures instructions (MSD Gold Sulfo-Tag NHS; Cat.# R91A0-1 and MSD Gold Sulfo-Tag NHS-Ester Conjugation Packs; Cat.# R31AA-1). MSD Streptavidin Gold plates (MSD; Cat.# L15SA-1)

were washed, blocked, coated with biotinylated Ab-1, and washed according the manufacture instruction. 50 ul of supernatant or standard were added to the plate and incubated overnight at 4 °C while shaking. Plates were washed 3 times and detection antibody was added and incubated for 2 hrs while shaking at room temperature. Plates were washed and read buffer added. Plates were read with a MSD reader Quick Plex S120.

Surface marker analyses by flow cytometry.

The expression of cell surface markers was analysed by staining for 15 min at room temperature (RT) in PBS supplemented with 0.5% (v/v) human serum (FACS buffer). To allow exclusion of dead cells, cells were stained prior to fixation using Fixable Viability Dye eFluor® 780 (eBioscience). Following fluorophore-conjugated antibodies were used for analysis (supplier, clone): anti-CD3 (BD Biosciences; UCHT1), anti-CD4 (Biolegend; RPA-T4), anti-CD8 (Biolegend; SK1), anti-CD14 (Biolegend; M5E2), anti-CD16 (Biolegend; 3G8), anti-CD19 (BD Biosciences; SJ25C1), anti-CD25 (Biolegend; MA-A251), anti-CD45RA (Biolegend; HI100), anti-CD56 (BD Biosciences; NCAM16.2), anti-HLA-DR (Biolegend; L243). For combined analysis of surface marker and intracellular cytokines, surface-stained cells where subsequently stained as described in the section Intracellular cytokine staining. Data were acquired on a LSRII flow cytometer (BD Biosciences).

Intracellular cytokine staining (ICCS).

Cells were stimulated in the presence of brefeldin A (BFA, 10 µg/ml, all from Sigma) for the final 4 hours of cell culture. Cells were fixed and permeabilised with Cytofix/Cytoperm (BD Biosciences) according to the manufacturer's instructions. To exclude dead cells from the analysis, cells were stained prior to fixation using Fixable Viability Dye eFluor® 780 (eBioscience). Following fluorophore-conjugated anti-cytokine antibodies were used for

analysis (supplier; clone): anti-IL-1α (Biolegend; 364-3B3-14), anti-IL-1β (Biolegend; H1b-98), anti-IL-4 (BD Biosciences; MP4-25D2), anti-IL-6 (eBioscience; MQ2-13A5), anti-IL-10 (Biolegend; JES3-9D7), anti-IL-13 (eBioscience: 85BRD), anti-IL-17A (eBioscience; eBio64DEC17), anti-IL-23p19 (eBioscience; 23dcdp), anti-GM-CSF (BD Biosciences; BVD2-21C11), anti-IFN-γ (eBioscience; 4S.B3), anti-TNF (Biolegend: MAb11). For the detection of IL-12p40 the combination of biotin-conjugated anti-IL-12p40 (BD Biosciences; C8.6) and streptavidin STV-CF594 (BD Biosciences; Cat.# 562318) were used. Data were acquired on a LSRII flow cytometer (BD Biosciences).

Monocyte cluster validation and tSNE analysis of flow cytometry data.

For the validation of scRNA-seq-identified monocyte clusters at the protein level, cells were stained for the following marker (supplier; clone): anti-CD14 (Biolegend; M5E2), anti-HLA-DR (Biolegend; L243), anti-CCL20/MIP-3 alpha (R&D; 67310), anti-CCL20/MIP-3 alpha (R&D; 114906), anti-IL-23p19 (eBioscience; 23dcdp), anti-CCL2 (eBioscience; 5D3-F7), anti-RPS6 (R&D; 522731), anti-SPINK1 (R&D; 839305), anti-IDO-1 (eBioscience; Eyedio), EBI3 (eBioscience; ebic6), anti-S100A8 (Invitrogen: CF-145), anti-S100A9 (Biolegend, MRP-14), anti-TNF (Biolegend: MAb11). Unconjugated antibodies targeting RPS6 and SPINK were conjugated in house using the Expedeon (Innova Biosciences) Lightning–Link PE/Texas Red or DyLight 405 antibody labelling kit according to the manufacturer's instructions, respectively. t-Distributed Stochastic Neighbor Embedding (TSNE)-based analysis was executed on FCS files compensated for spillover between channels and gated on live $CD3^{-}CD19^{-}CD56^{-}CD14^{+}$ single cells, down-sampled to 3.000 cells per sample. A single FCS file was generated by concatenating individual samples FCS files prior to tSNE unsupervised analysis using the FlowJo (Treestar) tSNE plugin[4,5] based on cluster defining genes. The following settings were used: Iterations = 1000; Perplexity = 200; Eta = 20; Theta

= 0.5. and included the following parameters: CD14, HLA-DR, CCL2, CCL20, IL-23p19, IDO-1, RPS6, SPINK1, S100A8 and TNF. Each individual analysis was performed on samples that were stained and acquired (LSRII (BD Biosciences)) on the same day.

IL-10 and IL-23 ELISpot assay.

ELISpot plates (Merck; Cat.#MSHAS4510) were incubated with sterile PBS (Gibco) and coated over night at 4°C with anti-IL-12/IL-23p40 (Mabtech; Cat.# MT86/221; 10 µg/ml in PBS) and anti-IL-10 (Mabtech; Cat.# 9D7;15 µg/ml in PBS) antibodies using 100 µl/well. On the next day plates were flicked and blocked using 100 µl/well 1x sterile PBS (Gibco) supplemented with 10% FCS (Sigma) for 2 hours at 37°C. Following, the buffer was removed and MACS-purified monocytes were plated at 2-fold concentration steps ranging from 6250 to 50.000 cells/well in complete RPMI medium supplemented with 10% FCS. Stimulation and incubation was performed over night at 37°C and 5% CO2 using combinations of LPS (200 ng/ml) and IL-10R blocking antibody (10 µg/ml). Following 16 hours incubation, cells were removed by flicking the plate and wells were washed extensively 10 times, each 1 minute incubation, with 200 µl washing buffer (0.1% Tween20 (Sigma) in PBS (Gibco). Secondary antibodies were diluted in PBS supplemented with 0.5% FCS (anti-IL-IL-23p19 (Mabtech; Cat.#/clone: MT155-HRP; 1 µg/ml) and anti-IL-10-biotin (Mabtech; Cat.#/clone: 12G8: 1 µg/ml). 100 µl/well antibody mixture was added to each well and incubation was performed for 2 hours at 37°C. Plates were then washed extensively 10 times, each 1 minute incubation. For the development of spots first 100 µl/well substrate solution (BCIP/NBT; Sigma) was added and development continued until distinct blue/grey spots emerged (approximately 5 minutes). Plates were again extensively washed 10 times, each 1 minute incubation, with 200 µl washing buffer. Then 100 µl/well substrate solution (AEC; BD Pharmingen) was added to each well and development was continued until distinct red

spots emerged (approximately 5 minutes). Plates were left to dry in the dark and images were acquired using an AID EliSpot Reader Systems. The anti-IL-10 clone 12G8 was conjugated with biotin (Novus Biologicals Lightning-Link Rapid Type A Biotin Antibody Labeling Kit).

Analysis of cytokine-induced STAT3 phosphorylation by flow cytometry.

Whole blood (Δ*IL10RA*) or PBMC (Δ*IL10RB*) were surface stained with anti-CD3-PE-Cy5 or anti-CD3-FITC (Biolegend; clone: UCHT1), anti-CD4-BV605 (Biolegend; clone: OKT4), anti-CD8-PE-CF594 (BD Biosciences; clone: RPA-T8), anti-CD14-BV650 (Biolegend; clone: M5E2), and anti-CD19-BV711 (BD biosciences; clone: HIB19 or clone: SJ25C1) for 20 min. Five minutes through surface staining, cells were stimulated with 100 ng/ml human recombinant IL-10 or IL-6 (Peprotech) for 15 min. Cells were subsequently fixed in pre-warmed (37°C) BD Cytofix for 10 minutes (BD biosciences) at 37°C. After fixation, cells were permeabilised on ice with ice-cold Perm Buffer III (BD biosciences) and stained with anti-pSTAT3 (pY705)-Alexa Fluor 647 (4/P-STAT3, BD Phosflow) for 1 h at room temperature before acquiring on a LSRII flow cytometer (BD Biosciences). For the analysis of IL-10 responsiveness in stimulated monocytes, cells were washed (2 times) in RPMI (Sigma) and incubated in RPMI for 2 hours. Following incubation, cells were washed (2 times) in RPMI and stimulated for 15 minutes in complete RPMI with 50 ng/ml recombinant human IL-10 (Preprotech). Cell were then stained in PBS (Sigma) on ice with Fixable Viability Dye eFluor® 780 (eBioscience). Subsequently, cells were fixed, permeabilised and stained as described above.

Generation and pre-processing of single-cell RNA-sequencing data.

$CD14^+$ monocytes were purified from PBMC by MACS positive selection (Mitenyi Biotec) according to the manufacturers' instructions from 2 human donors. The purity of sorting and

viability was assessed by surface staining and flow cytometry (anti-CD14 (Biolegend; M5E2); Fixable Viability Dye eFluor® 780 (eBioscience). Cells were plated in 96-well U-bottom plates at a cell density of $0.5x10^6$ cells/well in 200 µl complete RPMI and were left unstimulated or exposed to combinations of ultrapure 200 ng/ml LPS (Enzo Life Sciences; Cat.# ALX-581-008) and 10 µg/ml anti-IL-10R (Biolegend; clone: 3F9) for 16 hours. For droplet-based single cell RNA-sequencing analysis cells were collected in RPMI with L-glutamine (Sigma) supplemented with 0.5% human serum (Sigma; Cat.# H4522) and the cell number was adjusted to 1000 cells/µl. Single cell suspensions were kept on ice, washed in PBS with 0.04% BSA and resuspended. 10.000 single cells/channel were captured in droplets on Chromium 10x Genomics platform (less than one hour following the termination of stimulation). Library generation for 10x Genomics v2 chemistry was performed following the Chromium Single Cell 3′ Reagents Kits User Guide (CG00052). Quantification of library was performed using an Agilent Bioanalyzer and Bioanalyzer High Sensitivity DNA Reagents (Cat.# 5067-4627). Single-cell RNA-sequencing libraries were generated using the 10x Genomics Single Cell 3’ Solution (version 2) kit and sequenced to a minimum mean depth of 44.3k reads/cell (Illumina HiSeq 4000). An average of 2850 cells/per sample and 1150 genes/cell were recovered. Data analysis was performed using Python3 pipelines (https://github.com/sansomlab/tenx) written using the CGAT-core library #https://doi.org/10.12688/f1000research.18674.1. Read mapping, quantitation and aggregation of sample count matrices was performed with the 10x Genomics Cell Ranger pipeline (version 2.1.1) and version 1.2.0 (GRCh38) reference sequences. No normalisation was applied during the aggregation step. Cells with barcodes common to samples sequenced on the same lane(s) were removed from the analysis to avoid issues associated with index hopping. Aggregated count matrices were randomly down-sampled in order to normalise the median number of UMIs per-cell between the samples ("downsampleMatrix" function from

the DropletUtils R package). Down-sampling was performed separately for the within-donor cross-condition analysis (**Figure 3**) and the cross-donor analysis of LPS + anti-IL10R stimulated monocytes (**Supplementary Fig. 4b**).

Cross-condition analysis of single-cell RNA-sequencing data from a single donor. The dataset was filtered to remove cells with <500 genes, >5% mitochondrial reads per cell or that expressed lymphocyte markers (*CD3*, *CD79A* or *CD79B*, n=33 cells) leaving a total of n=2420 unstimulated, n=3149 LPS stimulated and n=2273 LPS + anti-IL-10R stimulated monocytes. Per-cell UMI counts were then normalised, scaled and the effects of total UMI counts, percentage of mitochondrial counts and cell cycle ("all" effects; using known G2 and S phase associated genes[6]) regressed out with the Seurat R package (version 2.3.4). Significantly variable genes (n=1164) were selected using the "trendVar" function from the R Bioconductor package Scran (minimum mean log-expression 0.05, BH adjusted p-value < 0.05). These genes were used as input for principal component analysis (PCA), and significant PCs (n=33) identified using Seurat ("JackStraw" test, BH adjusted p < 0.05). These principle components were used as input for alignment with Harmony (version 0.0.0.9, theta = 0). The first 30 Harmony components were used for graph-based clustering as implemented in Seurat ("original" Louvain algorithm, resolution=0.5). Significant cluster markers were identified using the Seurat "Findmarkers" function (Wilcoxon tests, BH adjusted p value < 0.05). The tSNE projection (Figure 3a) was computed using the 30 Harmony components and a perplexity of 50. Geneset over-representation analysis of cluster marker genes (Supplementary Fig. 4a) was performed using one-sided Fisher's exact tests (as implemented in the "gsfisher" R package https://github.com/sansomlab/gsfisher) with Biological Process gene sets obtained from the Gene Ontology (GO) database[7]. For this analysis cluster-specific gene universes were defined as those genes expressed in 10%

percent of cells (either within or outside the cluster of interest). Genesets were independently filtered for an odd ratio of ≥ 1.5 and n ≥ 3 foreground genes before multiple testing correction (enrichments with a BH adjusted $p < 0.05$ were considered significant).

Comparison of LPS + anti-IL-10R single-cell RNA-sequencing data from two donors. The dataset was filtered as for the cross-condition analysis (removing n=23 contaminating lymphocytes) and an equal number (n=2280) of cells randomly sub-sampled from each donor for further analysis. Normalisation and scaling (including regression of cell-cycle effects), identification of variable genes (n=849), identification of significant PCs (n=35) and clustering (resolution=0.6) was performed as described above (no alignment performed).

Identification and characterisation of gene co-expression modules in the RISK cohort. RPKM expression values for the RISK cohort[1,8] were retrieved from GEO (GSE57945), upper-quartile normalised and log2(n+1) transformed. Prior to WGCNA analysis the dataset was filtered to retain (n=13,850) genes that had a transformed expression value ≥ 1.5 in > 10% of the patients. The WGCNA R package (version 1.66) was then applied as follows (i) data was cleaned using the "goodSamplesGenes" function (with parameters: minFraction=0.5, minNsamples=4, minNGenes=4, minRelativeWeight=0.1), (ii) outlying samples (n=11) were identified and removed using the "cutreeStatic" function (with parameters: cutHeight=110, minSize=20), (iii) adjacencies calculated with the "adjacency" function (parameters: type=signed_hybrid, power=5, corFnc=cor, corOptions use=p and method=spearman"), (iv) the topological overall matrix computed with the "TOMsimilarity" function (parameter TOMType=unsigned), (v) a dynamic tree cut performed with function "cutreeDynamic" (parameter deepSplit=2, pamRespectsDendro=FALSE, minClusterSize=30) and (vi) modules merged with the "mergeCloseModules" function

(parameter cutHeight=0.25). Genes assigned to modules were subject to geneset over-representation analysis as described for the single-cell RNA-sequencing analysis with gene categories obtained from the Gene Ontology (GO) database[9], KEGG pathways[10] and sets of cell type marker genes (xCell)[11]. Indicative monikers for the modules were manually assigned based on genes with high module membership (r > 0.8 with the module eigengene) as well as GO category, KEGG pathway and xCell marker enrichments (see Suplementary Table 4). The overlap of the identified WGCNA modules with IBD GWAS associated genes was performed using the associations reported by Ellinghaus *et. al.*[12] (Ellinghaus Supplementary Table 3a, n=156 genes) or by de Lange *et. al.*[13] (de Lange Supplementary Table 2). The associated genes from de Lange *et. al.* were conservatively filtered to retain only "implicated" genes or genes that originate from single-gene loci (n=89 genes, 48 of which overlap with the Ellinghaus *et. al.* set).

Identification and characterisation of an IL-10-responsive monocyte gene signature. The IL-10 regulated inflammatory monocyte gene signature (**Figure 5e**) was constructed from (i) genes that showed ≥ 3-fold higher expression in at least one of the three LPS + aIL10R clusters than was found in any of the unstimulated or LPS-stimulated clusters (single-cell RNA-sequencing analysis, **Figure 3a**), (ii) genes that showed significantly higher expression in the $CD14^+$ positive PBMC fraction upon with anti-IL-10R + LPS stimulation versus LPS stimulation alone (n=1, IL-1B, **Supplementary Fig. 5**), and (iii) two genes from the literature: CD14, a well-established monocyte type cell marker and OSM which is known to be expressed by inflammatory monocytes in human IBD and to drive colitis in the *Hh* + anti-IL-10R model[14]. The predictive ability of genes in the IL-10 regulated inflammatory monocyte signature was investigated in RNA-seq data from the RISK cohort and Affymetrix microarray data from the Janssen[15] (UC-cohort GSE12251, **Figure 5f**). The UC-cohort

GSE12251 includes data from atients with active UC that had a total Mayo score between 6-12 and an endoscopic sub-score of at least 2. The response to infliximab was defined as endoscopic and histologic healing in patients that underwent a second flex sigmoidoscopy with rectal biopsies 4 weeks after the first infliximab infusion in case of a single infusion and at 6 weeks if they received a loading dose of infliximab at weeks 0, 2 and 6. The UC-cohort GSE12251 microarray data was RMA normalised (R Bioconductor package "oligo") and annotated with data from the R Bioconductor "hgu133plus2.db" package (annotated probes and probes mapping to multiple gene symbols were excluded; signals from probes mapping to the same gene symbol were averaged). Predictive ability was assessed by computation of area under the precision recall curve (AUPRC) using the R PRROC library.

Gene expression analysis using real time PCR and expression array.

Total RNA was extracted from cultured cells, using the RNeasy Plus Mini Kit (Qiagen), according to the manufacturer's protocol. The RNA yield was determined by quantifying the samples on a Nanodrop ND1000 UV-vis Spectrophotometer. Complementary DNA (cDNA) was synthesized from 200 ng of total RNA and transcribed using the High Capacity cDNA Reverse Transcription Amplification Kit (Applied Biosystems) according to the manufacturer's instructions.

Real-time PCR.

Real-time PCRs were performed in 96-well plates using the PrecisionPLUS qPCR Mater Mix (Primer Design) and the CFX96 Touch Real-Time PCR Detection System machine (BIO-RAD). The expression of transcripts was normalized to expression of Large Ribosomal Protein (*RPLPO*). Data analysis was performed using the Cycles threshold (ΔΔCt) method and expressed as mRNA relative expression ΔΔCt. The following TaqMan probes (Applied

Biosystems) were used for qPCR analysis: *IL23A* (Hs00900828_g1), *IFNG* (Hs00989291_m1), *RPLPO* (Hs99999902_m1).

Gene array expression and statistical analysis.

Background correction and quantile normalization of the gene expression data obtained from the Affymetrix Human Transcriptome Array 2.0 (HTA2) platform were performed by the RMA method[16]. Each gene's expression was defined at the level of the "transcript cluster", which is the collection all probesets on the HTA2 platform that are located within a gene's annotated position in the genome. These gene positions were defined by the Affymetrix NetAffxTM NA34 release, which is based on the GRCh37 human reference genome. Differential expression at the gene-level was performed using the empirical Bayes method implemented in LIMMA{Ritchie:ef}controlling for donor in the model. Differential expression between a given stimulation vs. PBMC control contrast was considered at a Benjamini-Hochberg adjusted p-value < 0.05 and absolute fold change > 2. A heatmap was produced using the heatmap.2 function from the gplots package (R-3.4.2) to visualise the union of genes that were regulated in each stimulation vs. PBMC control contrast.

Gene Ontology and pathway enrichment analysis

Functionally grouped networks of terms and pathways were visualised and analysed using the Cytoscape (version 3.6.1) ClueGO (version 2.5.1) and CluePedia (version 1.5.1) plug-in[17]. The analysis was performed by accessing the reactome (https://reactome.org/), Gene Ontology QuickGO immunological processes (https://www.ebi.ac.uk/QuickGO/) and KEGG pathway databases (https://www.genome.jp/kegg/pathway.html). Only pathways with an adjusted enrichment p-value ≤ 0.05 were considered (Two-sided hypergeometric test, Bonferroni step down p-value correction). GO terms were grouped based on the highest

significance when more than 50% of genes or terms were shared. As reference the selected ontologies sets were used.

Statistical analysis

Statistical analysis was performed using Prism version 8.0 (GraphPad Software). Comparisons were calculated by two-way ANOVA test, followed by Dunnet post-test for multiple comparisons. Cell numbers and frequencies were compared by one-way ANOVA followed by kruskal-wallis post-test for multiple comparison corrections. The level of statistically significant difference was defined as $p \leq 0.05$.

Mathematical modelling of cytokine interactions.

We define a system of ordinary differential equations of the form $\frac{dx_i}{dt} = s_i \prod_u (1 + \alpha_{u,i} x_u) \prod_v (1 + \beta_{v,i} x_v)$, with x_i the concentration of TNF, IL-1α, IL-1β, IL-6, IL-10 or IL-23 over time, s_i the contribution of LPS, and $\alpha_{u,i}$ ($\beta_{u,i}$) the positive (negative) effect of cytokine u on the production rate of cytokine i. With additional time and/or dose dependent data, the model could be extended by including saturation of cytokine production (e.g. using Michaelis-Menten or Hill functions) or cytokine degradation. By minimizing the log likelihood, we fit the right-hand side of the equations to 1750 experimental data points, representing cytokine production rates by monocytes 16 hours after LPS stimulation. These rates were determined by intracellular flow cytometry in PBMC derived from healthy individuals, in the presence or absence of anti-IL-10R, and TNF, IL-1β, IL-6, IL-10, IL-23, IFNγ, anti-IFNγ, anti-IFNR1, anti-IL-1α, anti-IL-1β, anti-IL-1R1, anti-IL-6R, or anti-TNF (n=3-17). The frequency of cytokine (i.e. TNF, IL-1α, IL-1β, IL-6, IL-10 or IL-23) producing live $CD14^+$ cells multiplied by the mean fluorescence intensity of the respective cytokine producing cell population was taken as a measure of cytokine production

rate. All possible network configurations using a set of edges representing significant (paired Wilcoxon test, $p \leq 0.05$) direct cytokine interactions derived from this dataset were considered, and for each number of edges, an optimal model configuration was found. We did not model all 2^{31}-1 possible configurations explicitly, as the vast majority of configurations could be logically excluded based on a small subset of network configuration fits. It was found that all optimal models were nested, i.e. the list of optimal models can be obtained by iteratively adding edges to the model. As additional edges will always improve the model fit, we use the Akaike Information Criterion (AIC) to identify the fourteen-edge model as the model with an optimal balance between edge number and model fit. For two nested models that differ one edge, the AIC is equivalent to a likelihood ratio test (LRT, alpha=0.16) with one degree of freedom. Fitting and parameter identifiability analysis of the fourteen-edge model was done in the Matlab based modelling environment 'Data2Dynamics', using a deterministic trust-region approach combined with a multi-start strategy; data2dynamics.org[18].

Resources for data visualization

Gene and protein networks were visualized using Cytoscape 3.6.1: http://www.cytoscape.org/[19].

Gene ontology and pathway enrichments were analysed using the Cytoscape 3.6.1 plugin ClueGO: http://apps.cytoscape.org/apps/cluego[17].

Heatmaps for gene expression data visualisation were generated using the GENE-E or Morpheus tool from the Broadinstitute: http://www.broadinstitute.org/cancer/software/GENE-E/; https://software.broadinstitute.org/morpheus/.

References

1. Kugathasan, S. *et al.* Prediction of complicated disease course for children newly diagnosed with Crohn's disease: a multicentre inception cohort study. *The Lancet* **389,** 1710–1718 (2017).
2. Schulthess, J. *et al.* The Short Chain Fatty Acid Butyrate Imprints an Antimicrobial Program in Macrophages. *Immunity* (2019). doi:10.1016/j.immuni.2018.12.018
3. Sonnenborn, U. Escherichia coli strain Nissle 1917-from bench to bedside and back: history of a special Escherichia coli strain with probiotic properties. *FEMS Microbiol. Lett.* **363,** fnw212 (2016).
4. Maaten, L. V. D. & Hinton, G. Visualizing Data using t-SNE. *Journal of Machine Learning Research* **9,** 2579–2605 (2008).
5. Wallach, I. & Lilien, R. The protein–small-molecule database, a non-redundant structural resource for the analysis of protein-ligand binding. *Bioinformatics* **25,** 615–620 (2009).
6. Dominguez, D. *et al.* A high-resolution transcriptome map of cell cycle reveals novel connections between periodic genes and cancer. *Cell Research* **26,** 946–962 (2016).
7. Ashburner, M. *et al.* Gene ontology: tool for the unification of biology. The Gene Ontology Consortium. *Nat Genet* **25,** 25–29 (2000).
8. Haberman, Y. *et al.* Pediatric Crohn disease patients exhibit specific ileal transcriptome and microbiome signature. *J. Clin. Invest.* **124,** 3617–3633 (2014).
9. Harris, M. A. *et al.* The Gene Ontology (GO) database and informatics resource. *Nucleic Acids Research* **32,** D258–61 (2004).
10. Kanehisa, M., Furumichi, M., Tanabe, M., Sato, Y. & Morishima, K. KEGG: new perspectives on genomes, pathways, diseases and drugs. *Nucleic Acids Research* **45,** D353–D361 (2017).
11. Aran, D., Hu, Z. & Butte, A. J. xCell: digitally portraying the tissue cellular heterogeneity landscape. *Genome Biol.* **18,** 220 (2017).
12. Ellinghaus, D. *et al.* Analysis of five chronic inflammatory diseases identifies 27 new associations and highlights disease-specific patterns at shared loci. *Nat Genet* **48,** 510–518 (2016).
13. de Lange, K. M. *et al.* Genome-wide association study implicates immune activation of multiple integrin genes in inflammatory bowel disease. *Nat Genet* **49,** 256–261 (2017).
14. West, N. R. *et al.* Oncostatin M drives intestinal inflammation and predicts response to tumor necrosis factor-neutralizing therapy in patients with inflammatory bowel disease. *Nat. Med.* **23,** 579–589 (2017).
15. Arijs, I. *et al.* Mucosal gene signatures to predict response to infliximab in patients with ulcerative colitis. *Gut* **58,** 1612–1619 (2009).
16. Irizarry, R. A. *et al.* Summaries of Affymetrix GeneChip probe level data. *Nucleic Acids Research* **31,** e15–e15 (2003).
17. Bindea, G. *et al.* ClueGO: a Cytoscape plug-in to decipher functionally grouped gene ontology and pathway annotation networks. *Bioinformatics* **25,** 1091–1093 (2009).
18. Raue, A. *et al.* Data2Dynamics: a modeling environment tailored to parameter estimation in dynamical systems. *Bioinformatics* **31,** 3558–3560 (2015).
19. Shannon, P. *et al.* Cytoscape: a software environment for integrated models of biomolecular interaction networks. *Genome Res.* **13,** 2498–2504 (2003).